NBS TECHNICAL NOTE

416

# Study of a Halpern-Type $4\pi$ Neutron Detector

H. M. Gerstenberg and E. G. Fuller


U.S. DEPARTMENT OF COMMERCE
National Bureau of Standards

# THE NATIONAL BUREAU OF STANDARDS

The National Bureau of Standards[1] provides measurement and technical information services essential to the efficiency and effectiveness of the work of the Nation's scientists and engineers. The Bureau serves also as a focal point in the Federal Government for assuring maximum application of the physical and engineering sciences to the advancement of technology in industry and commerce. To accomplish this mission, the Bureau is organized into three institutes covering broad program areas of research and services:

**THE INSTITUTE FOR BASIC STANDARDS** . . . provides the central basis within the United States for a complete and consistent system of physical measurements, coordinates that system with the measurement systems of other nations, and furnishes essential services leading to accurate and uniform physical measurements throughout the Nation's scientific community, industry, and commerce. This Institute comprises a series of divisions, each serving a classical subject matter area:

—Applied Mathematics—Electricity—Metrology—Mechanics—Heat—Atomic Physics—Physical Chemistry—Radiation Physics—Laboratory Astrophysics[2]—Radio Standards Laboratory,[2] which includes Radio Standards Physics and Radio Standards Engineering—Office of Standard Reference Data.

**THE INSTITUTE FOR MATERIALS RESEARCH** . . . conducts materials research and provides associated materials services including mainly reference materials and data on the properties of materials. Beyond its direct interest to the Nation's scientists and engineers, this Institute yields services which are essential to the advancement of technology in industry and commerce. This Institute is organized primarily by technical fields:

—Analytical Chemistry—Metallurgy—Reactor Radiations—Polymers—Inorganic Materials—Cryogenics[2]—Office of Standard Reference Materials.

**THE INSTITUTE FOR APPLIED TECHNOLOGY** . . . provides technical services to promote the use of available technology and to facilitate technological innovation in industry and government. The principal elements of this Institute are:

—Building Research—Electronic Instrumentation—Technical Analysis—Center for Computer Sciences and Technology—Textile and Apparel Technology Center—Office of Weights and Measures—Office of Engineering Standards Services—Office of Invention and Innovation—Office of Vehicle Systems Research—Clearinghouse for Federal Scientific and Technical Information[3]—Materials Evaluation Laboratory—NBS/GSA Testing Laboratory.

---

[1] Headquarters and Laboratories at Gaithersburg, Maryland, unless otherwise noted; mailing address Washington, D. C., 20234.

[2] Located at Boulder, Colorado, 80302.

[3] Located at 5285 Port Royal Road, Springfield, Virginia 22151.

UNITED STATES DEPARTMENT OF COMMERCE
Alexander B. Trowbridge, Acting Secretary
NATIONAL BUREAU OF STANDARDS • A. V. Astin, Director


# TECHNICAL NOTE 416

ISSUED JUNE 12, 1967

## Study of a Halpern-Type 4 $\pi$ Neutron Detector

H. M. Gerstenberg and E. G. Fuller

Radiation Physics Division
Institute for Basic Standards
National Bureau of Standards
Washington, D.C., 20234



For sale by the Superintendent of Documents, Government Printing Office
Washington, D.C., 20402 - Price 30 cents

Contents

# Study of a Halpern-Type 4π Neutron Detector

H. M. Gerstenberg and E. G. Fuller

The response to various neutron spectra of a 2-inch diameter $BF_3$ proportional counter in a Halpern-type geometry has been studied as a function of moderator thickness. Neutron sources used were a calibrated RaDBe(α,n) source and a series of photoneutron sources using a number of bremsstrahlung spectra. The reactions used were: $^{16}O(\gamma,n)$, $^{31}P(\gamma,n)$ and $d(\gamma,n)$. For these sources absolute neutron yields were determined either from the residual β+ activity or from the known cross section and the absolute bremsstrahlung intensity. Using these empirical data a final detector with 13 $BF_3$ counters was constructed. Over the spectral range covered by the above sources the measured efficiency for counting neutrons of the final detector was 9.6 percent with an estimated uncertainty of ±0.5 percent, independent of spectrum. The detector was used to measure the neutron yields from Pb, Au, Ta, Ho, Ag, Cu, Co, Ca, P, Al, O and C for a series of bremsstrahlung energies between 12.0 and 29.0 MeV. These yields were compared with those calculated from previously published neutron yield cross sections. The data indicate that previously reported discrepancies in neutron yield data can probably be traced to the determination of neutron detector efficiencies.

Key Words: Detector, efficiency, four-pi, Halpern, neutron, photoneutron, response, yields.

## 1. Introduction

The study of photonuclear interactions by measurements of photoneutron cross sections has been very fruitful. This is primarily because the photoneutron cross section represents a large percentage of the total absorption cross section; the percentage ranges from about 50% for the light elements to about 90% for the heavier elements such as lead. Of almost equal importance, however, is the fact that neutrons weakly interact with matter. This allows the use of thick targets and compensates for the relatively low photon yield available from accelerators such as the betatron.

Unfortunately, the magnitude of the photoneutron cross sections, as measured in different laboratories, show differences of as much as 30%. The problem may be due, in part at least, to the detectors used to measure the photoneutron yields. The most commonly used system is a relatively simple 4π neutron detector which moderates and then captures the neutrons emitted from the target. It is possible that variations in the designs of these detectors resulting in non-uniform responses as a function of neutron energy may have caused the discrepancies in the measured neutron cross sections.

Halpern, Mann and Nathans [1][1] were the first to design a 4π neutron detector for use with photoneutron experiments. Their system was designed on the basis of data by Rossi and Staub [2]

1 Figures in brackets indicate the literature references at the end of this paper.

which showed that for a $BF_3$ counter placed in the center of a large paraffin cube, it was possible to choose a moderator thickness between the counter and a source, such that the counting efficiency would be reasonably insensitive to neutron energy. The basic design of the Halpern detector consisted of a $BF_3$ counter embedded in a 2 ft x 2 ft x 3 ft paraffin block. The photon beam from the betatron passed through a one-inch diameter beam tube running through the center of the block parallel to the long dimension. The sample to be irradiated was placed at the center of the beam tube. The neutrons from the target were moderated by 3.8 inches of paraffin before being detected by counters mounted parallel to the beam tube. The axial separation of the source and counters used by Halpern, Mann and Nathans was the same as that recommended by Rossi and Staub but the intervening paraffin thickness was not the same due to differences in the counter diameters. Apparently, Halpern, Mann and Nathans felt that the distance between the source and counters was more important than the moderator thickness. Fast et al. [3] used the same source-counter axial separation but since even smaller $BF_3$ counters were used the intervening paraffin thickness was 4.1 inches. Other experimenters have used various moderator spacings between the target and counters. Spicer et al. [4] used 5.1 inches of moderator. In a later experiment by Baglin, Thompson and Spicer [5], the distance was changed to 3.9 inches of moderator. In a yet later experiment by Allum, Crawley and Spicer [6], a moderator distance of 2.76 inches was used. At all these distances, the detector was thought to have a detection efficiency independent of the initial energy of the emitted photoneutrons.

Attempts [7,8] have been made to determine the ideal moderator distance for a Halpern-type detector by using calculated or measured slow neutron flux distributions in paraffin produced by neutron sources having different energy spectra. Data of this type usually apply to an ideal geometry situation, i.e., point detectors at some distance from a point source. They are difficult to apply to the design of a Halpern-type detector which has one or more long cylindrical counters at some distance from a finite-sized neutron source or target. In these detectors the moderator thickness is usually considerably less than the dimensions of the sensitive volume of the $BF_3$ counters used. While the calculation of the detector response for a single geometrical arrangement of beam tube and counter undoubtedly could be carried out using Monte Carlo techniques, the problem of optimizing the geometrical arrangement to give a high efficiency which at the same time was independent of neutron energy appeared to be quite formidable. It was, therefore, decided to determine empirically the parameters influencing the response of a Halpern-type detector. On the basis of these empirically determined data, a detector was designed to have an efficiency insensitive to neutron energy. After calibration of the detector, it was then used to determine a number of bremsstrahlung-produced neutron yields.

## 2. Experimental Detail

An experimental arrangement was designed so that the response of a $BF_3$ counter could be studied as a function of the amount of moderator between the counter and a beam tube containing a source of neutrons. Beam tubes of various diameters could be used and the counter position could be adjusted to keep the moderator thickness constant. Fig. 1 shows this arrangement. It consisted of a large aluminum container through which a beam tube passed parallel to the long dimension. Mineral oil was chosen over paraffin as a moderator because it allowed parameters to be changed with a minimum of trouble. The results for either moderator should be the same as the hydrogen-carbon ratio is the same and the difference in density is less than 3%. The neutron background was reduced by a 0.25 inch boral* shield placed on the inside of the container walls. In addition, a minimum thickness of 10 inches of borax surrounded the outside of the container.

A total of 13 counters was used in the measurements. They all had very similar characteristics as is shown in Table 1 which gives the relative counts observed in each of the counters when exposed to RaDBe($\alpha$,n) source under identical conditions of geometry, anode voltage, amplifier gain, and discriminator bias. The rms deviation of the counts listed in Table 1 is 0.65% or only twice the deviation expected if the counters were identical.

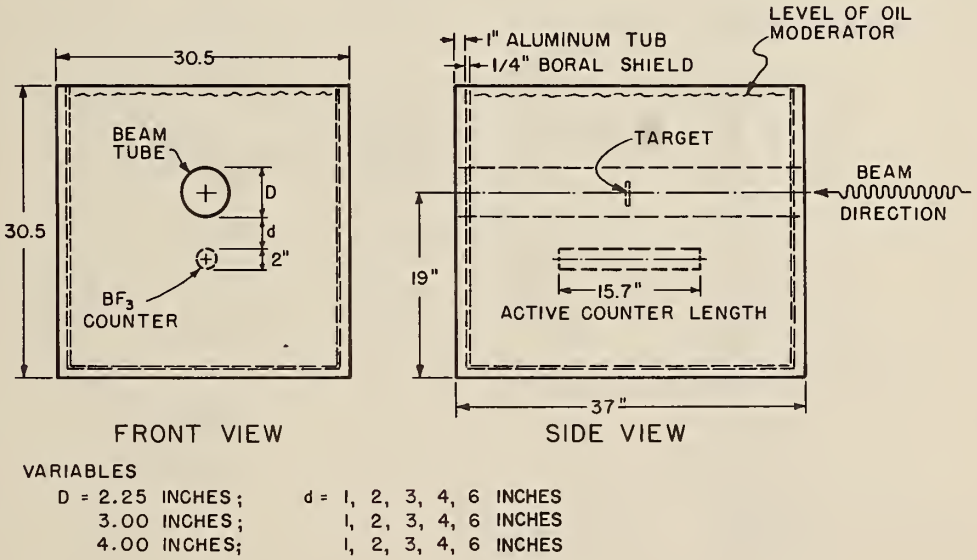


Fig. 1. The experimental arrangement used to study the response of the $BF_3$ counters. The counters, of which only one is shown, were placed at various distances d from a beam tube having a diameter D; mineral oil moderator was used to fill the aluminum tub.

* Aluminum with a uniform dispersion of boron carbide crystals.

Table 1. Comparison of $BF_3$ counters. The statistical uncertainty $(1/n)^{\frac{1}{2}}$, for any given counter, is of the order of 0.4%.

| Counter Number | Relative Counts |
|---|---|
| 1181 | 1,241 |
| 2001 | 1,251 |
| 1997 | 1,240 |
| RH526 | 1,226 |
| 2002 | 1,249 |
| 2167 | 1,235 |
| 2000 | 1,243 |
| 1178 | 1,247 |
| 1177 | 1,256 |
| 1179 | 1,248 |
| 1180 | 1,253 |
| 1999 | 1,239 |
| TB542 | 1,246 |

The counters used in the arrangement had an active length of 15.7 inches and a diameter of two inches. The filling pressure for the boron trifluoride was 70 cm of mercury and the boron was enriched to greater than 90% in $^{10}B$. The anode voltage applied to the counters was 3500 volts with measured plateaus approximately 400 volts long. Fig. 2 shows a typical voltage plateau. With a given source and beam tube diameter, measurements were made simultaneously for counters distributed about the beam tube with five different thicknesses of moderator (d = 1,2,3,4, and 6 inches) between the tube and counter.

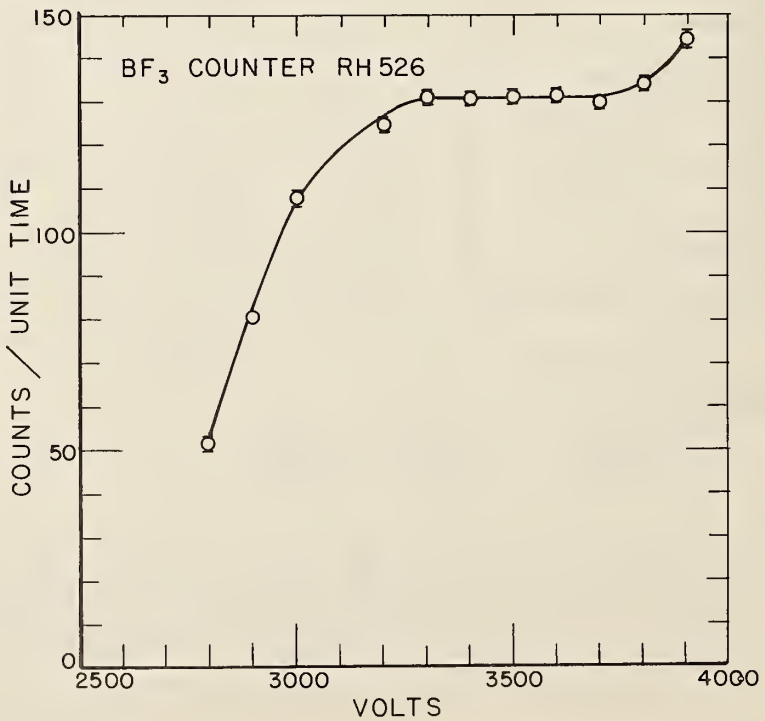


Fig. 2. The plateau for a typical $BF_3$ counter.

Three different beam tube diameters were used: D = 2.25, 3.0, and 4.0 inches. The counters at each moderator thickness were connected to separate counting channels. Each channel had one counter except the channels for d = 4 inches and 6 inches which contained 2 and 3 counters, respectively.

A block diagram of the electronics involved is shown in Fig. 3. A signal from a $BF_3$ counter, in one of the five channels, was fed into a preamplifier and then into an amplifier and a discriminator. The output pulse of the discriminator passed through a cathode follower to the experiment room. If the pulse passed through the gate, it was recorded on the scalars as a count in one of the $BF_3$ counters at a given position of d. An oscilloscope was used to display the relative time positions of the photon yield pulse, gate opening and closing, and the discriminator pulses due to neutrons.

For all measurements a gate width of 700 μsec was used to decrease the background counts. With the gate opening 10 μsec before the yield pulse, 98% of the neutrons detected were counted.

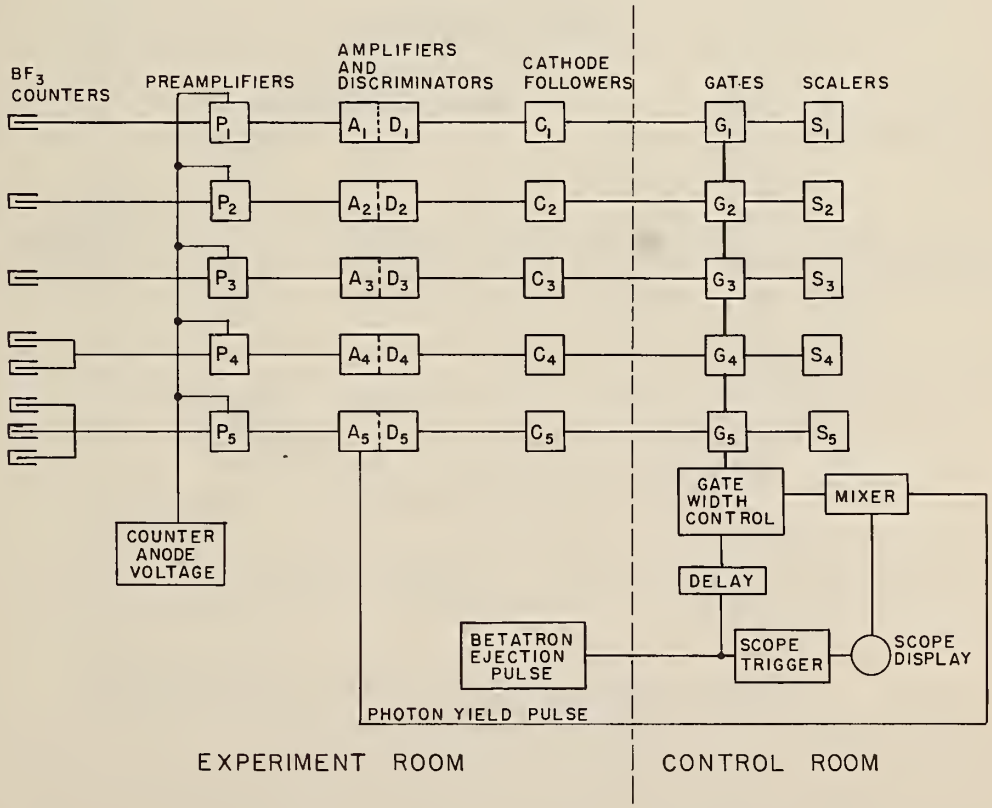


Fig. 3. Block diagram of the electronics. A total of five separate counting channels was used.

This procedure was preferable to having the gate open after the yield pulse since in the latter case uncertainties in the gate factor could be as high as 5%. This point is further discussed in Section IV. Each counter close to the beam tube had its own counting system. This was done to minimize yield pulse pile-up which could register as a false neutron count. In addition, care was used to insure that the peak of the photon yield burst was always less than the discriminator bias at the highest yield rate used.

The amplifiers were a non-overloading type with a maximum possible gain of 9,000. Delay line clipping was used at the input of the amplifier in order to obtain a well-shaped output pulse. The discriminator bias was set by measuring integral discriminator curves and biasing in a region of the counting plateau. Fig. 4 shows a typical integral discriminator curve.

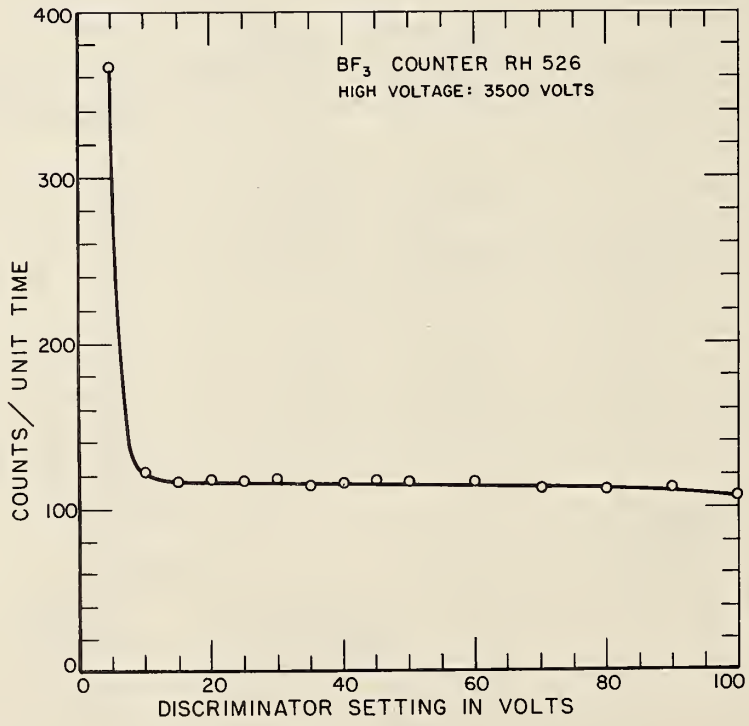


Fig. 4. A typical integral discriminator curve for a $BF_3$ counter.

The experimental arrangement is shown in Fig. 5. A photon beam, produced by a betatron, was collimated by a brass plug in a lead and nickel shielding wall. The beam then passed through the two lead collimators, a transmission monitor, and a final clean-up collimator, before striking a target located in the beam tube of the neutron detector.

The transmission monitor was a thin-wall, multi-plate, air ionization chamber with a total thickness of 5.66 $g/cm^2$ of aluminum. The charge created in the chamber was collected on capacitor plates. The voltage across the plates was measured with a vibrating reed electrometer. An absolute determination of the beam intensity was made by measuring the ionization charge collected from the transmission monitor and comparing it with the ionization charge collected from a standard NBS chamber [9]. The standard chamber is calibrated so that a measurement of the ionization charge collected during an x-ray exposure determined the total beam energy incident on the front face of the chamber.

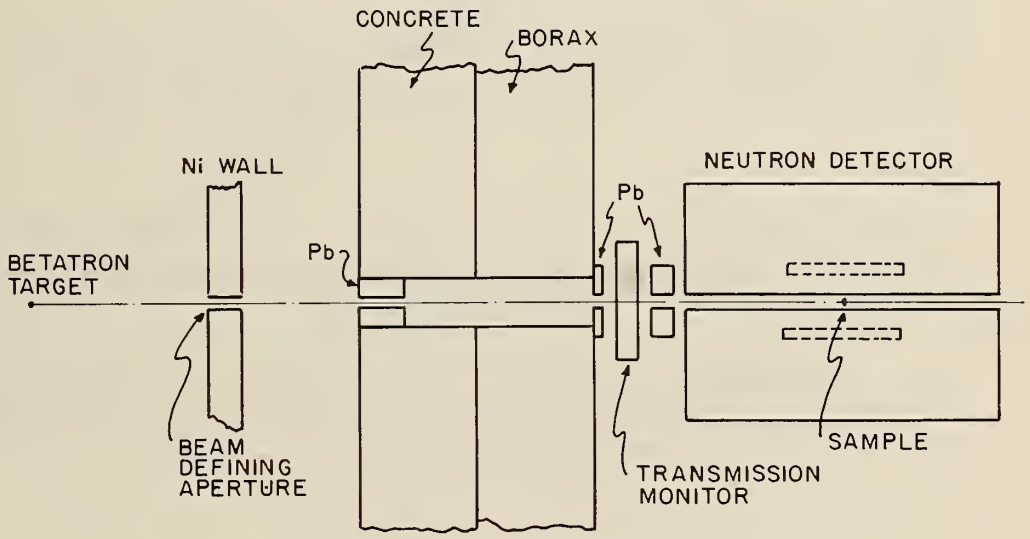


Fig. 5. The experimental arrangement. For all measurements the photon beam from the betatron was one inch in diameter at the sample position.

### 3. Neutron Sources

The counter efficiencies were determined for the detection of neutrons from a calibrated RaDBe($\alpha$,n) source and from three photoneutron sources made with bremsstrahlung. For the latter sources the neutron spectra were changed by varying the peak energy in the bremsstrahlung spectrum. The reactions used were: $D(\gamma,n)p$, $^{16}O(\gamma,n)^{15}O$, and $^{31}P(\gamma,n)^{30}P$.

Since in the decay of RaD($RaD \rightarrow {}^{210}Bi \rightarrow {}^{210}Po$) alpha particles are not emitted until $^{210}Po$ is reached, the ($\alpha$,n) source was considered to have the same neutron energy spectrum as a PoBe($\alpha$,n) source.

Representative spectra [10] measured for PoBe(α,n) sources are shown in Fig. 6. The different spectral shapes possibly result from variations in the geometry and construction techniques used to prepare the different sources.

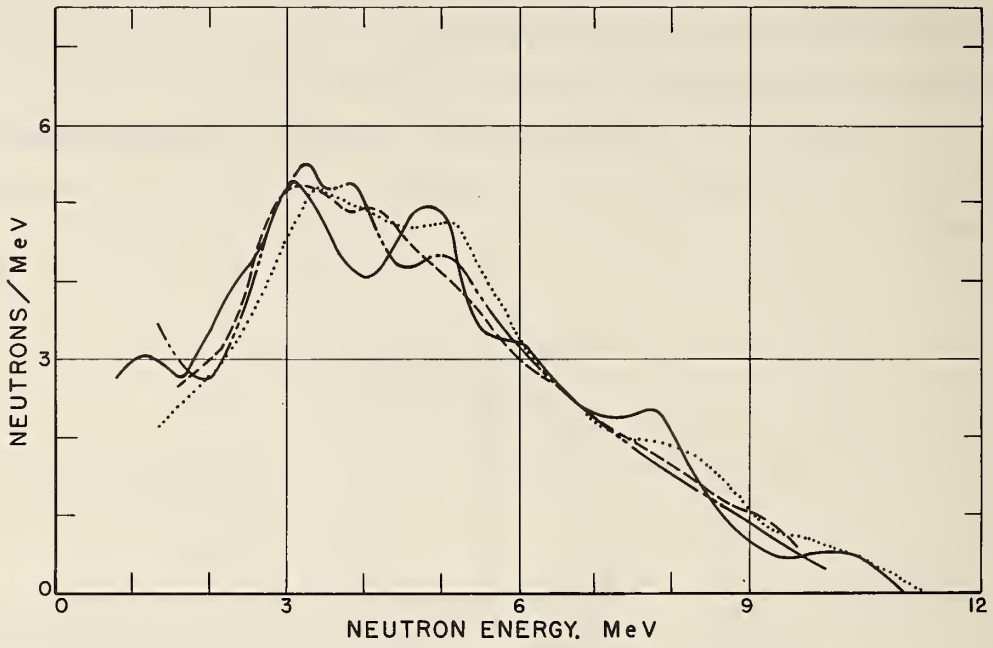


Fig. 6. Measured neutron energy spectra of various PoBe(α,n) sources are obtained from Ref. 10. The differences in the curves are assumed to be due to the methods of measurement and variations in the construction of the sources. It is assumed that the RaDBe(α,n) source used in this work has the same spectrum.

The energy spectrum for a photoneutron source depends on the photon (in this case bremsstrahlung) spectrum, the photonuclear cross section, and the level scheme of the daughter nucleus. Fig. 7 shows a typical bremsstrahlung spectrum as well as the cross section for the D(γ,n)p reaction. The spectrum, obtained from the Penfold-Leiss Tables [11], is corrected for attenuation by both the betatron doughnut wall and the transmission monitor. The cross section, obtained from a review article by Fuller and Hayward [12], is that calculated by Hulthen and Nagel [13] at the low energies and de Swart and Marshak [14] for energies above 10 MeV. In this particular case, where the reaction is strictly a two-body breakup and the residual nucleus has no level structure, there is a one-to-one relationship in the center-of-mass system between photon energy and neutron energy. For a thin deuterium target

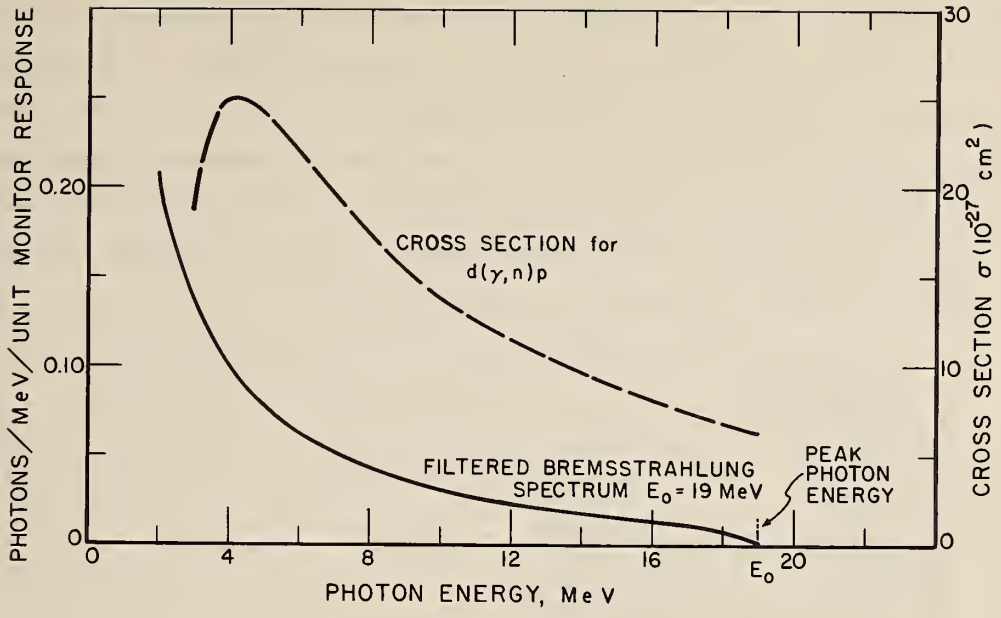


Fig. 7. The deuterium photodisintegration cross section and the incident photon spectrum. These curves were folded together to give the neutron spectrum from deuterium when operating the betatron at a peak bremsstrahlung energy of 19 MeV.

and a bremsstrahlung spectrum given by $I(E,E_o)/E$, the number of disintegrations by photons of energy E in the photon interval dE is proportional to $\sigma_d(E)\ I(E,E_o)dE/E$ where $E_o$ is the peak bremsstrahlung energy and $\sigma_d(E)$ is the cross section for the $D(\gamma,n)p$ reaction. If the momentum transferred by the photon is neglected, the normalized neutron energy spectrum is then given by:

$$N(E_n,E_o)dE_n = \frac{2\sigma_d(E)I(E,E_o)dE_n}{E\int_o^{E_o}\sigma_d(E)\frac{I(E,E_o)}{E}\,dE} \qquad (1)$$

where the neutron energy is given by $E_n = (E-2.22)/2$. The calculated energy spectrum of the neutrons for various peak bremsstrahlung energies is shown in Fig. 8. The spectrum of the RaDBe(α,n) source is also shown for comparison.

The (γ,n) reaction in $^{16}O$ was picked as a photoneutron source to use both because the cross section has a number of sharp peaks [15,16] which would result in well-defined neutron energy groups as well as because the daughter nucleus $^{15}O$, had a convenient half-life so that the induced radioactivity could be used to determine the absolute yield of neutrons. In this case, the (γ,n) reaction also proceeds by a two-body breakup. However, only for photons having energies below the threshold for the production of neutrons leaving $^{15}O$ in its first excited state is there a simple one-to-one relationship of photon energy to neutron energy.

Fig. 9 gives the total neutron yield cross section measured by Caldwell et al. [16]. Also shown is the cross section for leaving $^{15}O$ in its ground state. This latter cross section, taken from the work of Firk [17], has been normalized to the total neutron yield cross section over the photon energy range 20.5 - 21.5 MeV, i.e. near the threshold for transition to the 5.2 MeV states in $^{15}O$. (See energy level diagram at top of Fig. 9). Neutron counter efficiencies were determined for the neutron spectra produced by 18.0, 19.0, 20.0, 21.4, 22.4 and 24.5 MeV bremsstrahlung spectra. These peak energies are indicated by the arrows in Fig. 9.

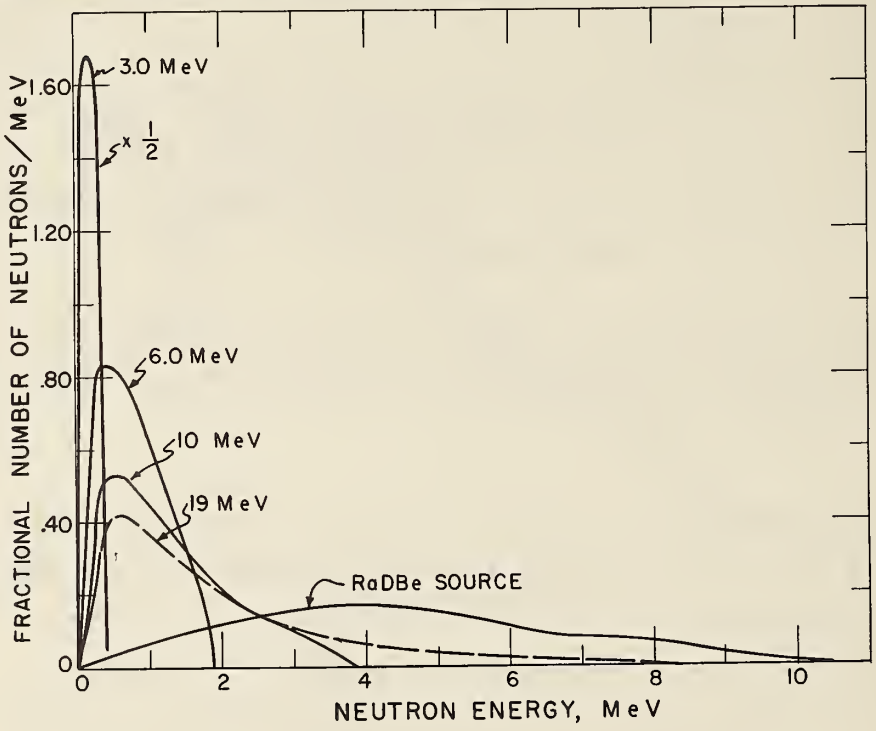


Fig. 8. Neutron energy spectra from a thin deuterium target. These curves were calculated for peak bremsstrahlung energies of 3.0, 6.0, 10.0, and 19.0 MeV. Also shown is the neutron spectrum from a RaDBe(α,n) source which was obtained by drawing a smooth curve through the data shown in Fig. 6.

Representative spectra of the photoneutrons from the oxygen source are given in Figs. 10, 11 and 12. The spectra in Figs. 10 and 11, where the peak bremsstrahlung energy is effectively below the threshold for the emission of neutrons leaving $^{15}O$ in the 5.2 MeV states, were calculated in the same way as those for the deuterium source. The spectrum produced by 27 MeV bremsstrahlung given in Fig. 12 is that measured by Firk [17].

The reaction $^{31}P(\gamma,n)^{30}P$ was chosen as a photoneutron source primarily because of its convenient half-life which made the determination of an absolute efficiency possible. In addition, it had been used for some of the original checks on the response of the Halpern-type detector. Neither detailed cross section nor neutron spectral data are available for energies up to the $(\gamma,2n)$ threshold. As a

result of the relatively high level density of $^{30}P$, it can probably be assumed that the spectrum is considerably softer than that of $^{16}O$.

The neutron emission rate of the RaDBe(α,n) source was determined in the NBS graphite pile by comparison with a secondary standard PuBe(α,n) source. The PuBe(α,n) source had been calibrated by comparison with the primary standard RaDBe(γ,n) source, NBS-1, in the NBS manganese sulfate bath. The size and description of the various sources used are given in Table 2.

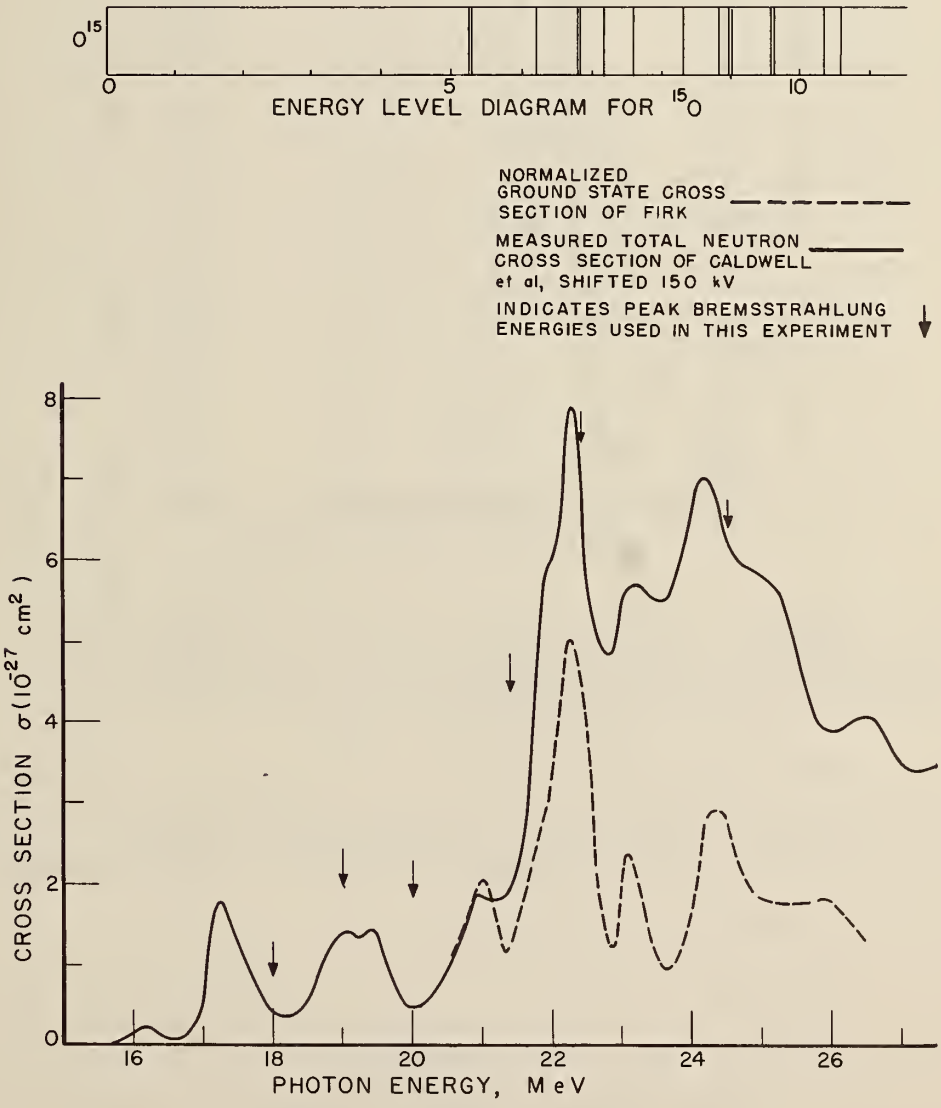


Fig. 9. Total neutron production cross section of $^{16}O$ and the cross section for the production of neutrons leaving $^{15}O$ in its ground state. The difference between the two gives the cross section for leaving $^{16}O$ in one of the excited states.

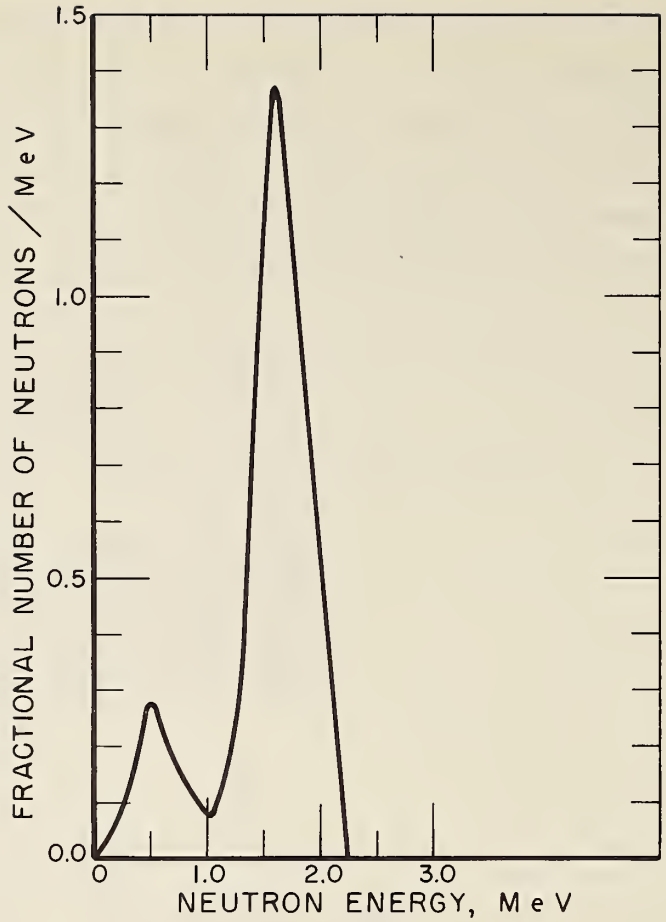


Fig. 10. Calculated neutron energy spectrum from $^{16}O$ for a peak bremsstrahlung energy of 18.0 MeV. This was obtained by folding the cross section for leaving the $^{15}O$ nucleus in the ground state with the filtered bremsstrahlung spectrum having a peak energy of 18.0 MeV.

An absolute detector efficiency, using the d(γ,n)p source, was obtained from the ratio of the measured neutron yield to the yield calculated from the known photodisintegration cross section, bremsstrahlung spectrum and an absolute measurement of the intensity of the bremsstrahlung beam. The efficiency of the neutron counters is then given by:

$$\varepsilon(E_o) = \frac{Y(E_o)\int_o^{E_o} I(E,E_o)\,dE}{n\varphi\int_o^{E_o} \sigma_d(E)\frac{I(E,E_o)}{E}\left[\frac{1-e^{-\mu t}}{\mu t}\right]dE} \qquad (2)$$

where $I(E,E_o)/E$, $\sigma_d(E)$, E and $E_o$ are the same as defined earlier; $Y(E_o)$ is the measured neutron yield in terms of the total energy in the beam; n is the number of target nuclei/cm$^2$; $[1-\exp(-\mu t)]/\mu t$

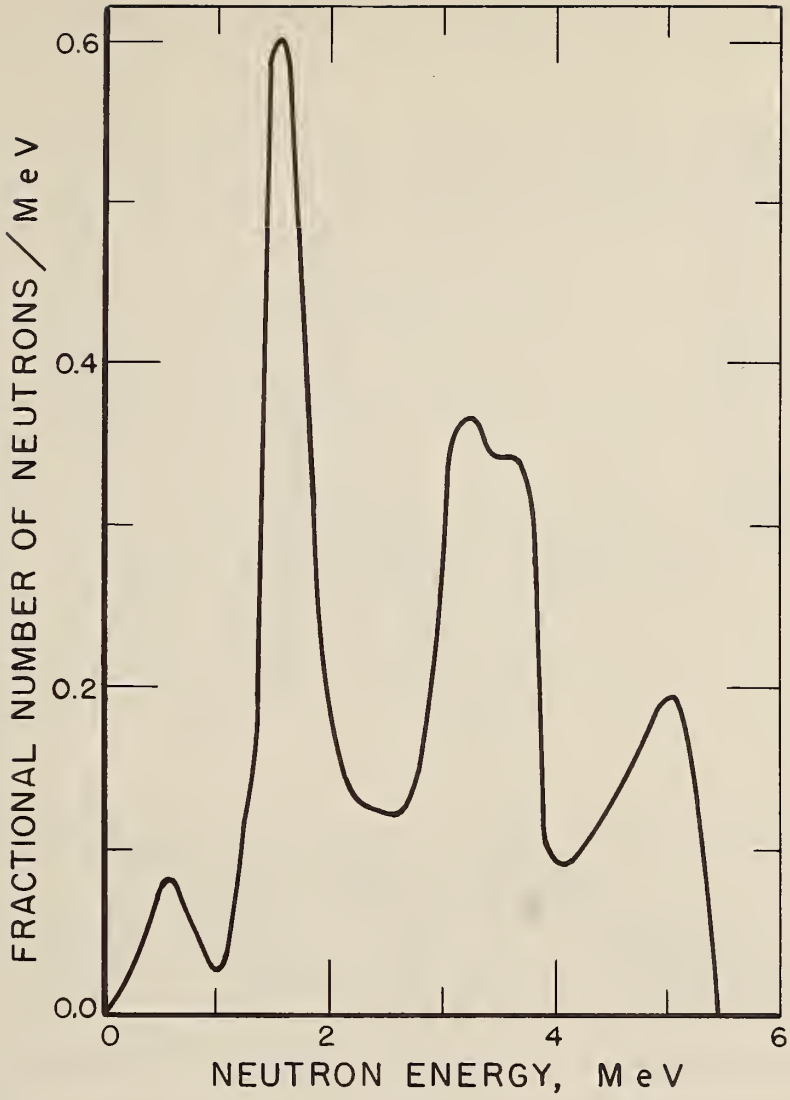


Fig. 11. Calculated neutron energy spectrum from $^{16}O$ for a peak bremsstrahlung energy of 21.4 MeV. See caption of Fig. 10 for details.

is the correction factor used to obtain the effective target thickness; $\mu$ is the photon attenuation coefficient in $cm^2/g$; t is the target thickness in $g/cm^2$; and $\varphi$ is the gate factor or the ratio of neutrons counted with a gate to neutrons counted without a gate. It was realized that the counter efficiency also depended on the extent of neutron moderation and absorption occurring in the targets themselves. This is discussed further in Section V.

The detector efficiency for the $^{16}O$ and $^{31}P$ sources was determined from the ratio of the neutron counting rate to the neutron production rate resulting from a constant betatron output.

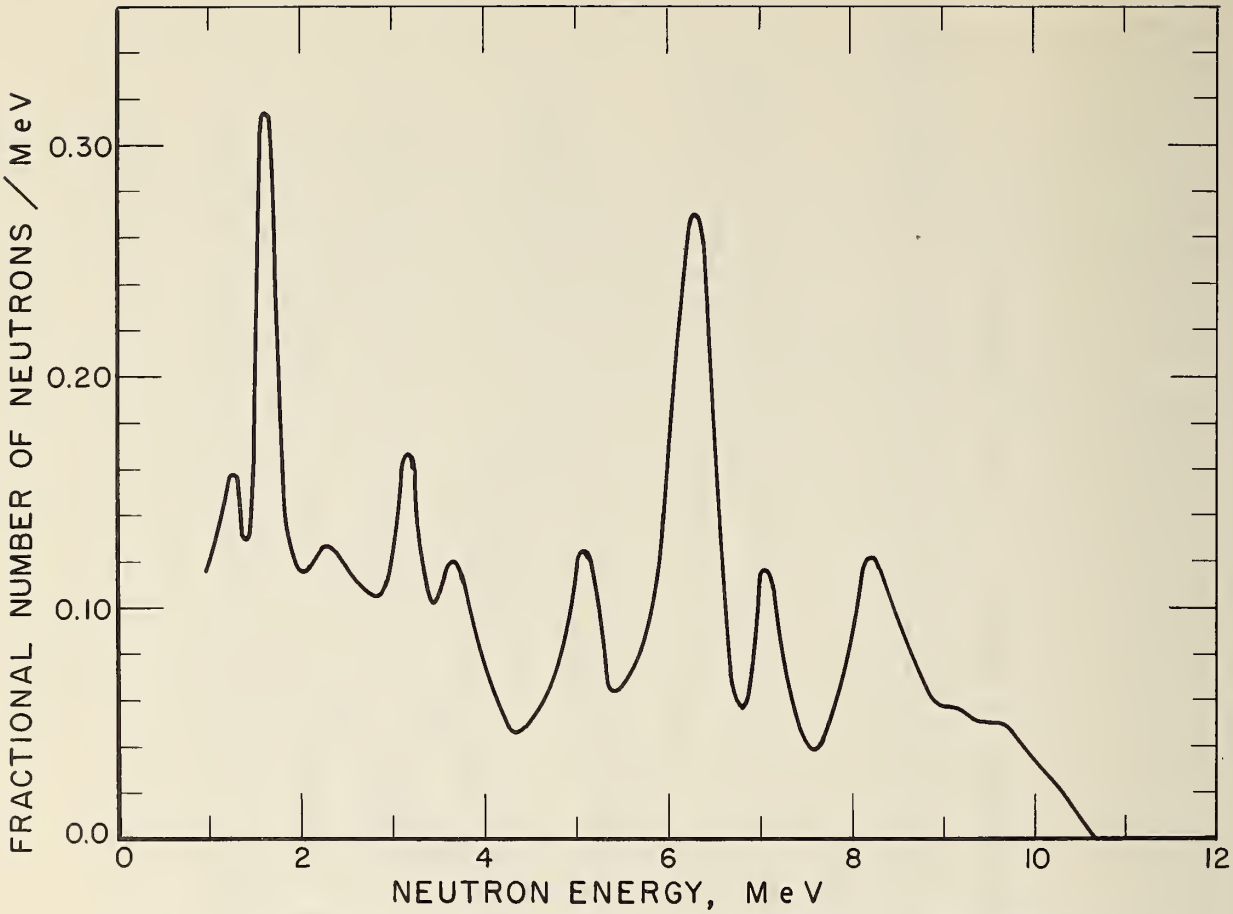


Fig. 12. The measured photoneutron spectrum from $^{16}O$ produced by 27 MeV bremsstrahlung. Due to uncertainties in the response function of the detector used in these measurements the spectrum shape below about 2 MeV is in some doubt.

The absolute neutron production rate for each run was determined from a measurement of the absolute positron disintegration rate of the sample bombarded. Each run was monitored in terms of the equilibrium voltage developed across a "leaky" capacitor that was charged by the ionization current from the transmission monitor. The plates of the capacitor were shorted through a resistor whose value was chosen such that the RC time constant of the monitoring circuit was equal to the mean life for decay of the positron activity induced in the samples by the $(\gamma,n)$ reaction.

A schematic diagram of the time sequence used for absolute calibration of the $^{16}O$ and $^{31}P$ sources is shown in Fig. 13. The beam was turned on at $t_o$ and the sample irradiated until an equilibrium decay rate $I_c$ was reached at $t_1$. A total neutron count, N, was then recorded in the period from $t_1$ to $t_2$. The irradiation was stopped at $t_3$ and the sample placed in a NaI(Tl) well crystal calibrated for absolute positron counting. Between $t_4$ and $t_5$ a total positron count, $\eta$, was measured. This positron count is given by:

$$\eta(E_o) = \varepsilon(\beta+) \int_{t_4}^{t_5} I_c(E_o) e^{-\lambda t} dt = \frac{\varepsilon(\beta+) I_c(E_o)}{\lambda} \left[ e^{-\lambda t_4} - e^{-\lambda t_5} \right] \quad (3)$$

where $\varepsilon(\beta+)$ is the positron detection efficiency of the NaI crystal and $\lambda$ is the positron decay constant of the target. The total number of neutrons detected by the neutron counters in the time interval $t_2 - t_1$ is:

$$N(E_o) = \varphi \varepsilon(E_o) I_c (t_2 - t_1) \quad (4)$$

where $\varepsilon(E_o)$ is the efficiency of the neutron counters and $\varphi$ is the gate factor. Using Equation 3 in Equation 4, $\varepsilon(E_o)$ is given by:

$$\varepsilon(E_o) = \frac{\varepsilon(\beta+) N(E_o)}{\lambda \varphi \eta(E_o)} \left[ \frac{e^{-\lambda t_4} - e^{-\lambda t_5}}{t_2 - t_1} \right] \quad (5)$$

Typical values for the parameters and constants are shown in Table 3.

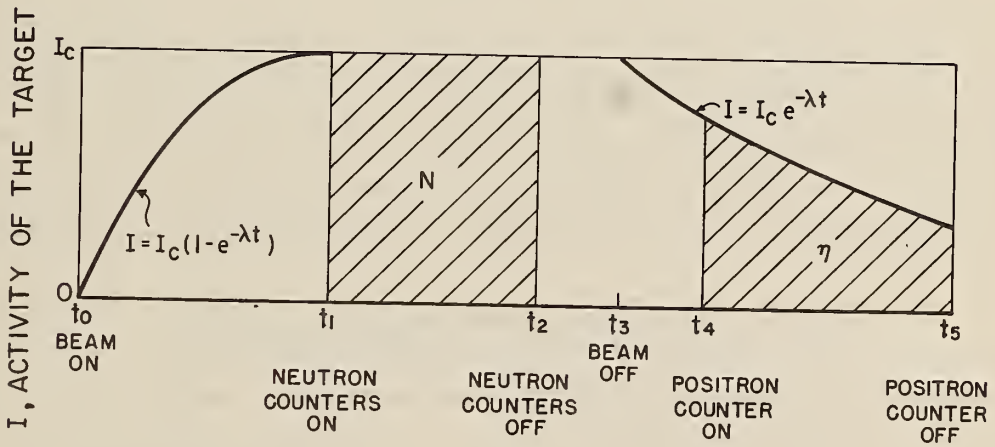


Fig. 13. Schematic of the time sequence used for the calibration of the $^{31}P$ and $^{16}O$ sources. N is the total neutron counts recorded by the scalers in the time interval $t_2$-$t_1$ and $\eta$ is the total positron counts recorded by the positron counter in the time interval $t_5$-$t_4$.

Table 2. Size and description of sources used for calibration of the neutron detector

| Source | Absolute Calibration | | | Relative Calibration | | |
|---|---|---|---|---|---|---|
| | Diameter (inches) | Length (inches) | Description | Diameter (inches) | Length (inches) | Description |
| $d(\gamma,n)p$ | 2.0 | 2.75, 2.00, 1.00, 0.50, & 0.20 | $D_2O$ contained in thin-wall aluminum cylinders | 2.0 | 2.75 | $D_2O$ contained in a thin-wall aluminum cylinder |
| $^{16}O(\gamma,n)^{15}O$ | 0.58 | 0.88 | $H_2O$ contained in a thin-wall plastic cylinder | 0.65 | 2.75 | $H_2O$ contained in a thin-wall plastic cylinder |
| $^{31}P(\gamma,n)^{30}P$ | 0.58 | 0.88 | Red phosphorous contained in a thin-wall plastic cylinder | 0.65 | 2.75 | Red phosphorous contained in a thin-wall plastic cylinder |
| RaDBe($\alpha$,n) | 0.35 | 0.35 | RaDBe($\alpha$,n) sealed in a metal cylinder | | | |

The peak photon energy produced by the betatron was controlled by a system [18] based on the determination of the average magnetic field in the vicinity of the electron orbit at the instant of x-ray production. The field was sampled by a search coil whose signal was proportional to the time rate of change of field. The signal was integrated and the integrator output was a voltage analog of the field, i.e., proportional to the electron's momentum. A discriminator was set to fire when this

Table 3. Typical values for the constants and parameters used to obtain the neutron counter efficiencies.

| Parameter or Constant | Value |
|---|---|
| $\lambda(^{15}O$ source) | $5.634 \times 10^{-3}$ $(sec)^{-1}$ |
| $t_2 - t_1$ | 10.0 min |
| $\epsilon(\beta^+)$ | 0.83 |
| $t_5 - t_4$ | 260 sec |
| $t_4 - t_3$ | 20 sec |
| $\varphi$ | 0.98 |

voltage reached a predetermined value. The ejection pulse to the expander coils of the betatron was timed manually such that the betatron yield pulse and discriminator pulse from the integrator were coincident in time; this condition insured that x-ray production occurred at the predetermined magnetic field value.

The energy calibration of the betatron was based on $(\gamma,n)$ reaction thresholds and positions of peaks in the $^{16}O(\gamma,n)^{15}O$ cross section. An analysis of the calibration indicated that the standard deviation for the peak bremsstrahlung energy was less than 1% for all energies above 8 MeV. From the reproducibility of the counting rate it has been estimated that the betatron energy can be reset and maintained within 60 keV at 20 MeV [19].

## 4. Counter Efficiencies

The sources described in the previous section were used to determine the efficiency of a $BF_3$ counter placed in various geometries in the moderator container shown in Fig. 1. Measurements were made with a moderator thickness (d) of 1, 2, 3, 4, and 6 inches and with beam tube diameters (D) of 2.25, 3.00, and 4.0 inches. In the following section only the results obtained with D = 2.25 inches will be described in detail. A brief description is also given of the effects of neighboring counters and voids in the moderating bath.

The efficiency per counter for detecting the spectrum of neutrons resulting from the $d(\gamma,n)p$ reaction is given in Fig. 14 and Table 4 as a function of both the counter position in the moderating bath and the peak bremsstrahlung energy. While the two highest energy points plotted in Fig. 14 are above the $^{16}O(\gamma,n)$ threshold the magnitude of the bremsstrahlung weighted yield from this reaction is negligible compared with that from the deuteron reaction at these energies. The bar on each of the $d(\gamma,n)p$ points is the expected rms deviation due to uncertainties in the gate factor, the number of nuclei/$cm^2$, the calibration of the betatron energy, the absolute calibration of the photon beam intensity, the shape of the photon spectra, and the number of counts observed. There is an additional factor of ± 10% in all of these efficiencies arising from the uncertainty in the magnitude of the $d(\gamma,n)p$ cross section. These data have been corrected for the finite thickness of the $D_2O$ target by assuming that only a part of the Compton cross section was effective in removing photons from the bremsstrahlung beam. (See discussion on thick target effects in Section V).

The efficiencies indicated by the black dots to the right of Fig. 14 were determined with the RaDBe$(\alpha,n)$ source. These cannot be compared directly with the data obtained with the $D_2O$ source since no corrections have been made for the absorption of neutrons in the large volume of the $D_2O$ source. As an indication of the magnitude of this effect, when the RaDBe$(\alpha,n)$ source was mounted in the center of the $D_2O$ container the counting rate observed when the container was full of $D_2O$ or $H_2O$ was 0.93 times that observed when the container was empty. This measurement was made with 4 inches of moderator separating the counter from the beam hole. Note that with this sort of correction

applied to the data in Fig. 14, the efficiency of the counter with 4 inches of moderator is roughly insensitive to the spectrum emitted by the source. It should also be noted that the ratio of the efficiencies determined with the $D_2O$ and RaDBe(α,n) neutron sources is by no means independent of moderator thickness. This ratio gives, for a given moderator thickness, the magnitude of the factor by which photoneutron cross sections could be in error if the photoneutron spectra being detected differed markedly from the spectrum of the source used to calibrate the detector.

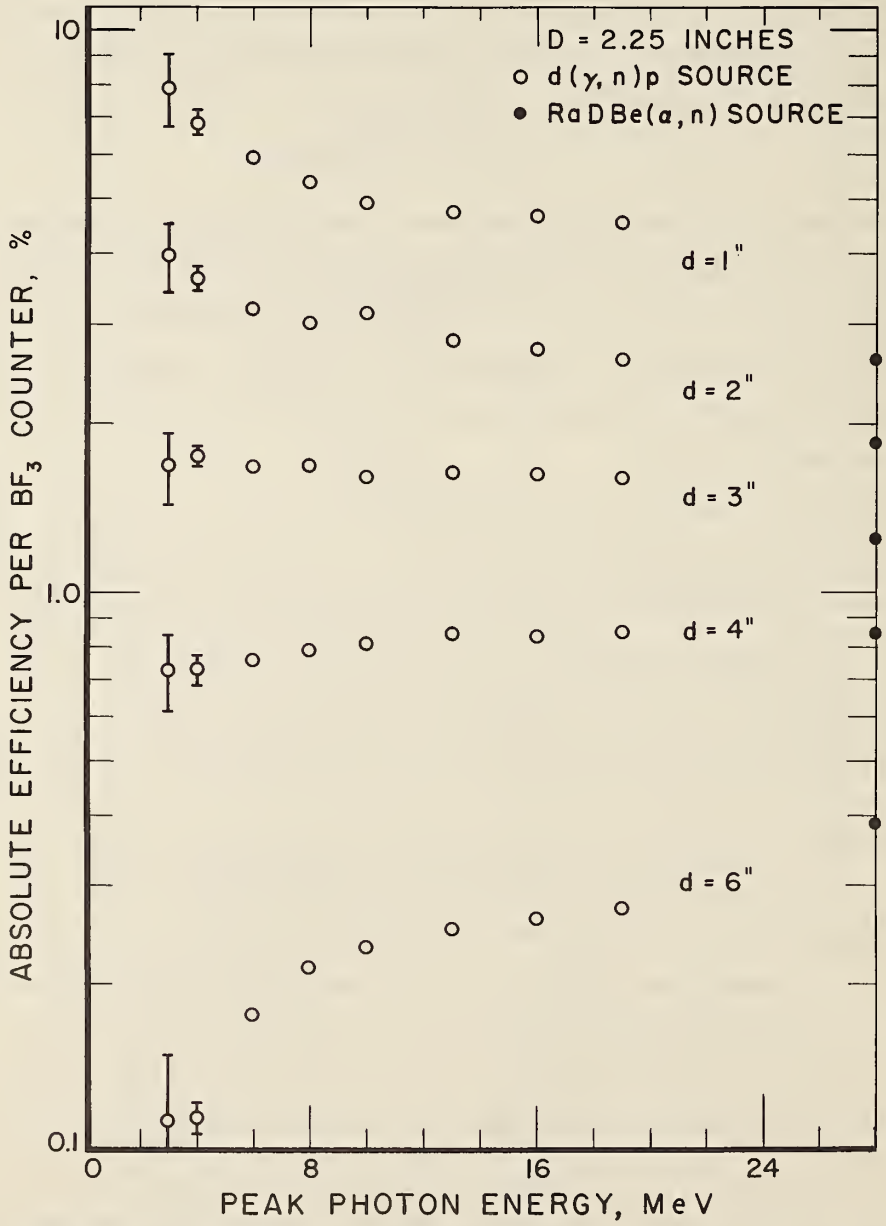


Fig. 14. Measured neutron counter efficiencies for the d(γ,n)p source as the peak photon energy is varied. Except where bars are shown, the uncertainties in the measurements are equal to or less than the size of the circles. The measurements were made with a beam tube diameter of 2.25 inches. These data have been corrected for the finite thickness of the $D_2O$ target by assuming that only a part of the Compton cross section was effective in removing photons from the bremsstrahlung beam.

Table 4. Neutron counter efficiencies for the d(γ,n)p source. The efficiencies as measured with the RaDBe(α,n) source are also shown. No correction has been made for the finite thickness of the target. The statistical uncertainties ($N^{\frac{1}{2}}$) only are indicated for each measurement.

| Beam Tube Diameter, D. (inches) | Peak Photon Energy, MeV | Counter Efficiency, o/o Moderator Thickness, d | | | | |
|---|---|---|---|---|---|---|
| | | 1.0 inches | 2.0 inches | 3.0 inches | 4.0 inches | 6.0 inches |
| 2.25 | (RaDBe) | 2.59±0.01 | 1.84±0.07 | 1.25±0.05 | 0.84±0.04 | 0.39±0.02 |
| " | 19 | 4.14 0.02 | 2.35 0.02 | 1.45 0.01 | 0.77 0.01 | 0.25 0.002 |
| " | 16 | 4.24 0.03 | 2.45 0.02 | 1.47 0.01 | 0.75 0.01 | 0.23 0.002 |
| " | 13 | 4.35 0.04 | 2.54 0.03 | 1.48 0.01 | 0.76 0.01 | 0.22 0.003 |
| " | 10 | 4.45 0.04 | 2.84 0.03 | 1.45 0.01 | 0.73 0.01 | 0.21 0.002 |
| " | 8 | 4.91 0.05 | 2.74 0.03 | 1.52 0.02 | 0.72 0.01 | 0.19 0.003 |
| " | 6 | 5.35 0.10 | 2.89 0.06 | 1.53 0.03 | 0.68 0.01 | 0.16 0.004 |
| " | 4 | 6.24 0.23 | 3.30 0.13 | 1.59 0.06 | 0.67 0.03 | 0.11 0.007 |
| " | 3 | 7.22 0.59 | 3.61 0.30 | 1.53 0.14 | 0.66 0.06 | 0.10 0.03 |
| 3.0 | (RaDBe) | 2.19±0.09 | 1.67±0.07 | 1.12±0.05 | 0.76±0.03 | 0.35±0.014 |
| " | 19 | 3.50 0.06 | 2.19 0.04 | 1.28 0.02 | 0.69 0.01 | 0.23 0.004 |
| " | 16 | 3.51 0.06 | 2.20 0.04 | 1.27 0.02 | 0.67 0.01 | 0.22 0.004 |
| " | 13 | 3.61 0.06 | 2.27 0.04 | 1.30 0.02 | 0.67 0.01 | 0.21 0.004 |
| " | 10 | 3.70 0.06 | 2.30 0.04 | 1.28 0.02 | 0.64 0.01 | 0.19 0.004 |
| " | 8 | 4.07 0.07 | 2.45 0.04 | 1.33 0.03 | 0.65 0.01 | 0.17 0.003 |
| " | 6 | 4.38 0.10 | 2.56 0.06 | 1.31 0.03 | 0.59 0.01 | 0.14 0.003 |
| " | 4 | 5.17 0.20 | 2.86 0.10 | 1.35 0.05 | 0.58 0.02 | 0.11 0.008 |
| " | 3 | 5.58 0.78 | 3.17 0.44 | 1.31 0.20 | 0.53 0.08 | 0.096 0.031 |
| 4.0 | (RaDBe) | 1.75±0.07 | 1.41±0.06 | 0.99±0.04 | 0.68±0.03 | 0.31±0.012 |
| " | 19 | 2.95 0.03 | 1.85 0.03 | 1.11 0.02 | 0.61 0.01 | 0.21 0.006 |
| " | 16 | 3.02 0.05 | 1.86 0.04 | 1.12 0.02 | 0.60 0.01 | 0.20 0.004 |
| " | 13 | 2.95 0.06 | 1.93 0.04 | 1.13 0.02 | 0.61 0.01 | 0.18 0.004 |
| " | 10 | 2.97 0.05 | 1.97 0.03 | 1.12 0.02 | 0.58 0.01 | 0.16 0.003 |
| " | 8 | 3.21 0.07 | 2.10 0.04 | 1.16 0.02 | 0.58 0.01 | 0.15 0.003 |
| " | 6 | 3.68 0.09 | 2.15 0.05 | 1.14 0.03 | 0.53 0.01 | 0.12 0.003 |
| " | 4 | 4.36 0.17 | 2.53 0.10 | 1.21 0.05 | 0.51 0.02 | 0.092 0.005 |
| " | 3 | 4.65 0.65 | 2.69 1.08 | 0.15 0.15 | 0.48 0.07 | 0.051 0.008 |

The neutron counter efficiencies for the $^{16}O(\gamma,n)^{15}O$ source are plotted as a function of peak bremsstrahlung energy in Fig. 15. The bar shown on each point for the $^{16}O(\gamma,n)^{15}O$ source represents the rms deviation expected as a result of the number of counts observed. The relative data plotted in Fig. 15 were all obtained with the large size water sample listed in Table 2. The points taken with the RaDBe(α,n) source have been normalized to the data taken with the oxygen sample for a moderator thickness of 4 inches. Note that in this case, in contrast with Fig. 14, the ratio of the efficiency determined at the higher bremsstrahlung energies to that determined with the RaDBe(α,n) source is independent of the amount of moderator between the beam tube and the counter. This is to be expected since the neutron energy spectra of the two sources are similar.

The relative neutron counter efficiencies for the $^{31}P(\gamma,n)^{30}P$ source are plotted versus peak bremsstrahlung energy in Fig. 16. The bar, as shown on each point, is the standard deviation due to uncertainties in the counting statistics as only a relative comparison is made. The general shape of the plots are more like those measured for the d(γ,n)p source but show less change in the

efficiency as the bremsstrahlung energy is varied. This indicates that the spectra are reasonably soft and do not change their average energy as the peak bremsstrahlung energy is changed. Note that again the ratio of the efficiency determined with the phosphorous source to that determined with the RaDBe(α,n) source is strongly dependent on moderator thickness.

The general features indicated in Figs. 14-16 for the dependance of counter efficiency on neutron spectral shape and moderator thickness were the same when measurements were carried out with beam tube dimensions of 3.0 and 4.0 inches.

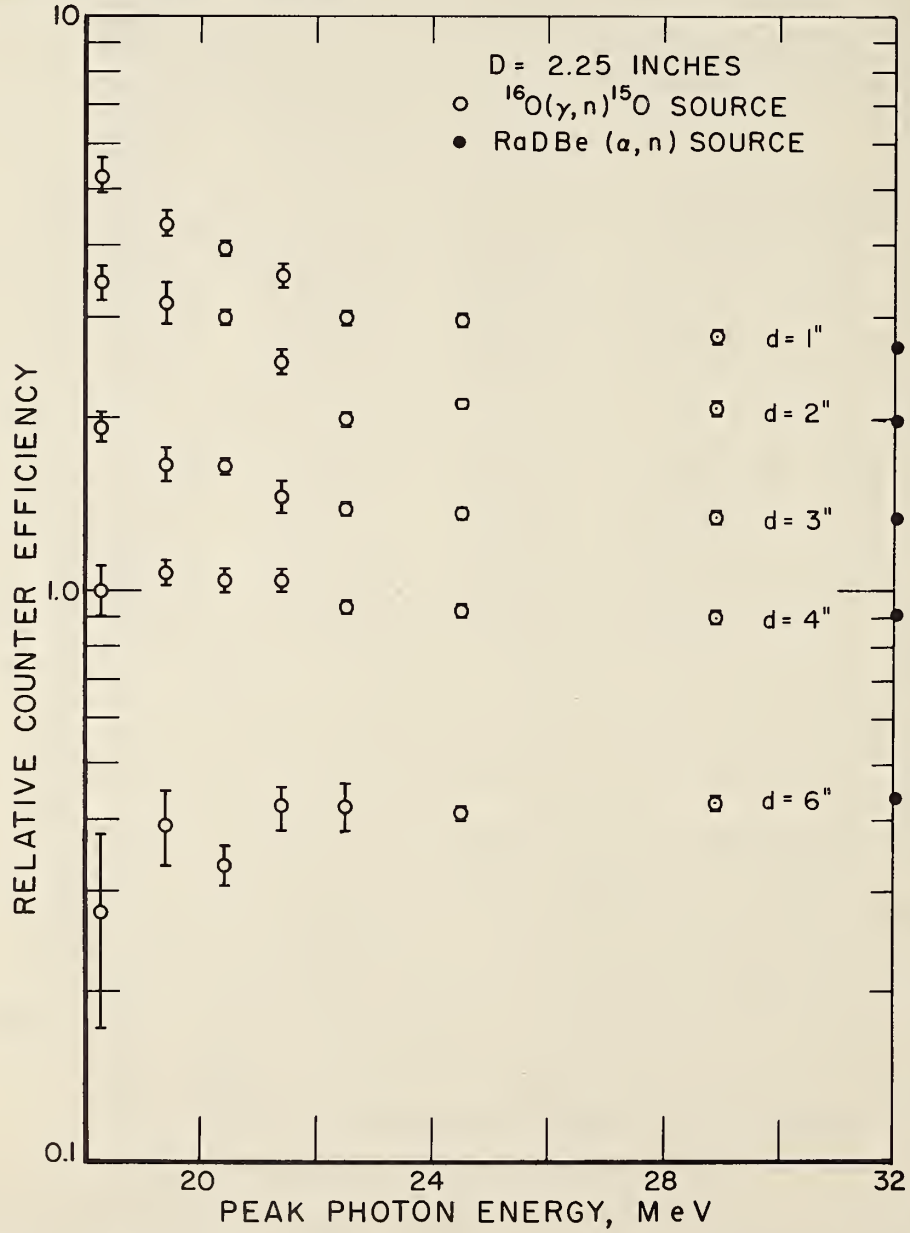


Fig. 15. Relative counter efficiencies for the $^{16}O(\gamma,n)^{15}O$ source as the peak photon energy is varied. The solid points are the measured counter efficiencies for the RaDBe(α,n) source. The two sets of data have been normalized together for a moderator thickness of 4 inches.

Neutron time distributions from lead and $D_2O$ targets were measured to determine if the gate factor (ratio of neutrons counted with a gate to neutrons counted without a gate) could in any way be influenced by the neutron spectra being measured. A beam tube diameter of 3.0 inches was used for the measurements made with the lead target at a peak bremsstrahlung energy of 18.0 MeV as well as for the $D_2O$ target at peak bremsstrahlung energies of 19.0 and 8.0 MeV. A beam tube diameter of 4.0 inches was also used with the $D_2O$ target at a peak bremsstrahlung energy of 19.0 MeV. These data were consistent with those obtained with the smaller beam tube.

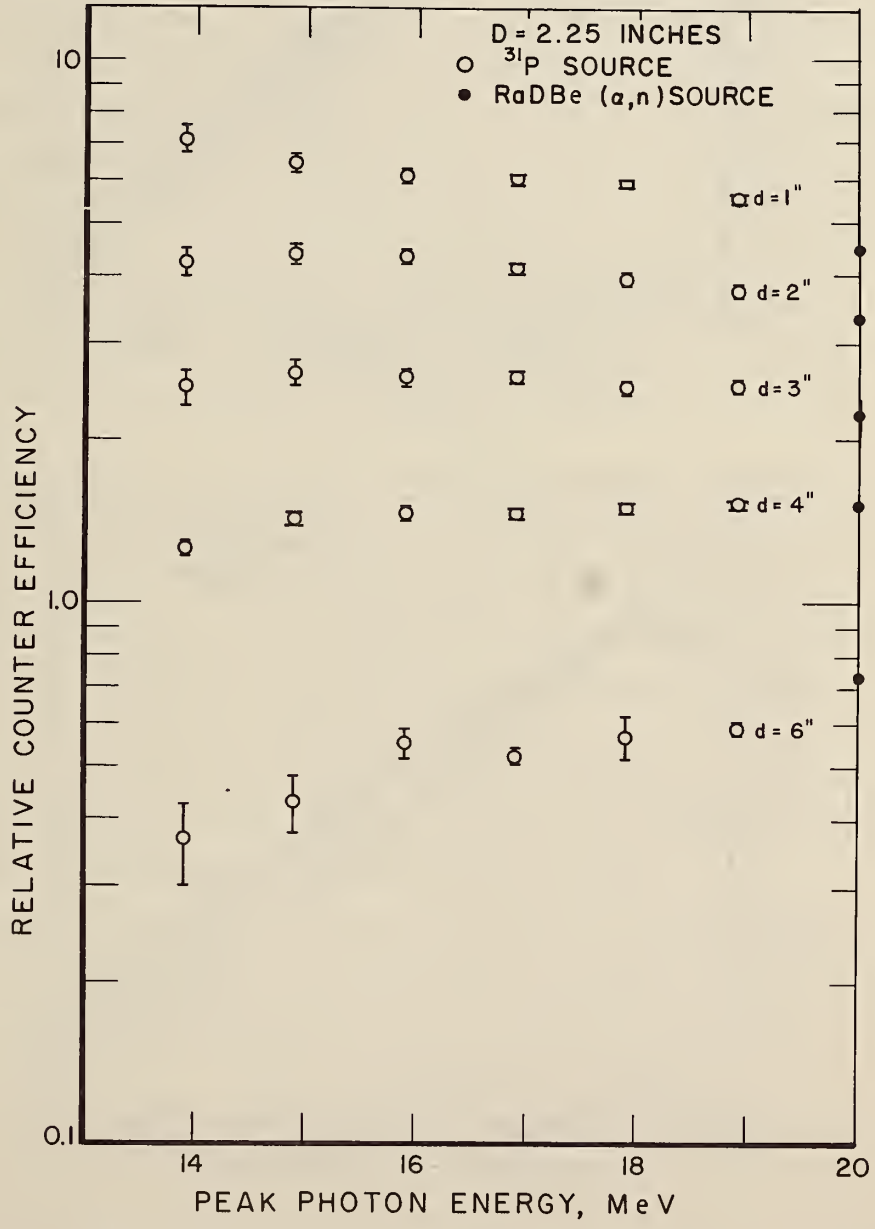


Fig. 16. Measured relative neutron counter efficiencies for the $^{31}P(\gamma,n)^{30}P$ source as the peak photon energy is varied. Data obtained with the RaDBe(α,n) source (indicated by solid circles) are normalized to the phosphorous data for a moderator thickness of 4 inches.

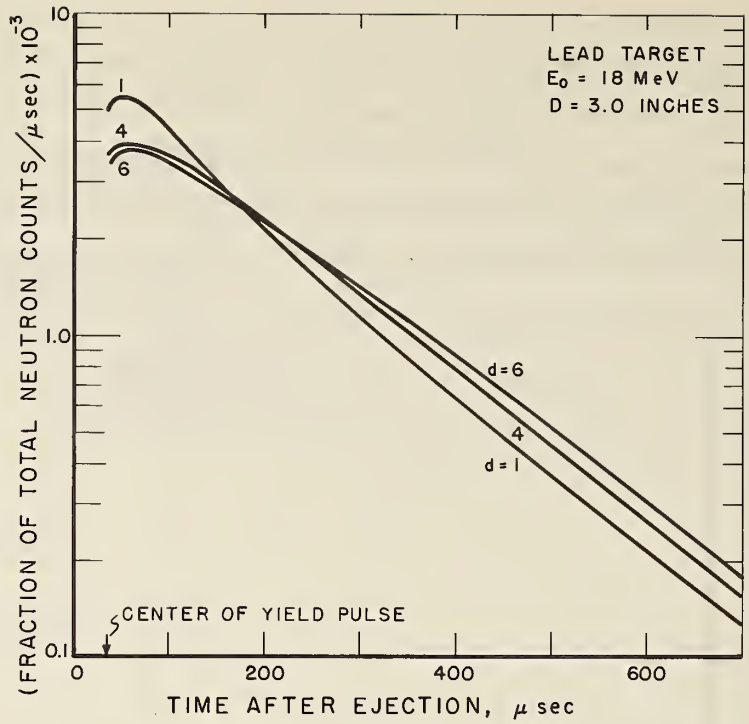


Fig. 17

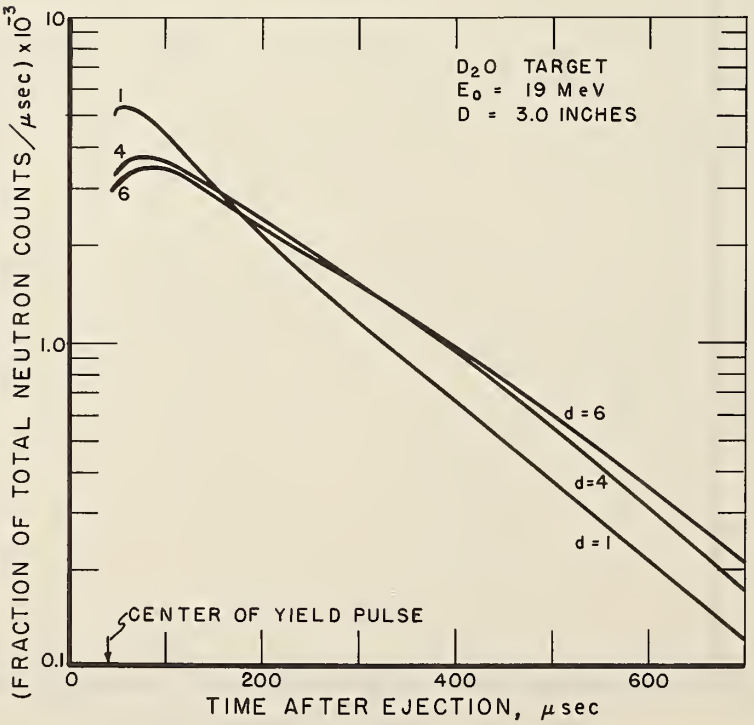


Fig. 18

Figs. 17 & 18. Neutron time distribution. See discussion in text.

Measurements were made by opening a gate, of a given width, at time intervals determined by a time marker generator triggered at zero time by the betatron ejection pulse. A gate with a width of approximately 10 μsec was positioned every 10 μsec for the first 100 μsec after the ejection pulse, a gate having a width of approximately 20 μsec was positioned every 20 μsec for the next 100 μsec, and a gate having a width of 100 μsec was positioned every 100 μsec for the time interval between 200 to 700 μsec. The data were recorded in counts per unit monitor response for a given gate width. The ungated counts per unit monitor response was then measured to obtain the fraction of total neutrons counted for a given gate width. The gate widths were determined by measuring at a known gate repetition rate the ratio of gated to ungated neutron counts from a RaDBe source. Using the measured gate widths, the fraction of total neutrons counted per μsec was then determined.

The data obtained from the measurements, in units of fraction of total neutrons counted per μsec, are plotted in Figs. 17-22. The beam pulse for these measurements had a rounded top and was about 15 μsec wide at the base. Figs. 17-19 are semilog plots giving the entire time distribution from zero to 700 μsec. Figs. 20-22 are linear plots showing the initial rise of the neutron counting rate. For clarity the individual data points are not given in these graphs. The smooth curves represent "best fits by eye" to the actual points. Statistical uncertainties ($N^{-\frac{1}{2}}$) were of the order of 2% for each point.

Although interpretation of the curves is made difficult because of poor geometry in the experiment, some general observations pertaining to their applications with the neutron detector can be made. The data in Figs. 17-19 which show the logarithmic decay of neutrons with time, can be fitted with essentially a straight line although the plots in general are convex downwards for a moderator thickness less than 4 inches and convex upwards for a moderator thickness greater than 4 inches. This effect has been observed before [20]. From these plots the half-life for the absorption of neutrons with time is found to be approximately 137 μsec for the counters with a moderator thickness of 4 inches. The counters with less moderator have a slightly shorter half-life for absorption while those counters with more moderator have a slightly longer half-life.

The time distribution of neutrons in Figs. 20-22 vary in both shape and magnitude depending upon the target, the peak bremsstrahlung energy and the moderator thickness d. A neutron counting system using a long gate (approximately 700 μsec), opening 20 μsec after the yield pulse, will be sensitive to these variations in the time distributions. As much as a 5% difference in the gate factor is obtained between the counters with one and 6 inches of moderator using a $D_2O$ target and a peak bremsstrahlung energy of 8.0 MeV; similar variations in the gate factor are found as the targets and peak bremsstrahlung energies are changed. This is understood by considering the time distributions in Figs. 20-22; the number of neutrons not counted by the gate is essentially the area under the curves from zero time to the time of the opening of the gate. Changes in these areas are reflected

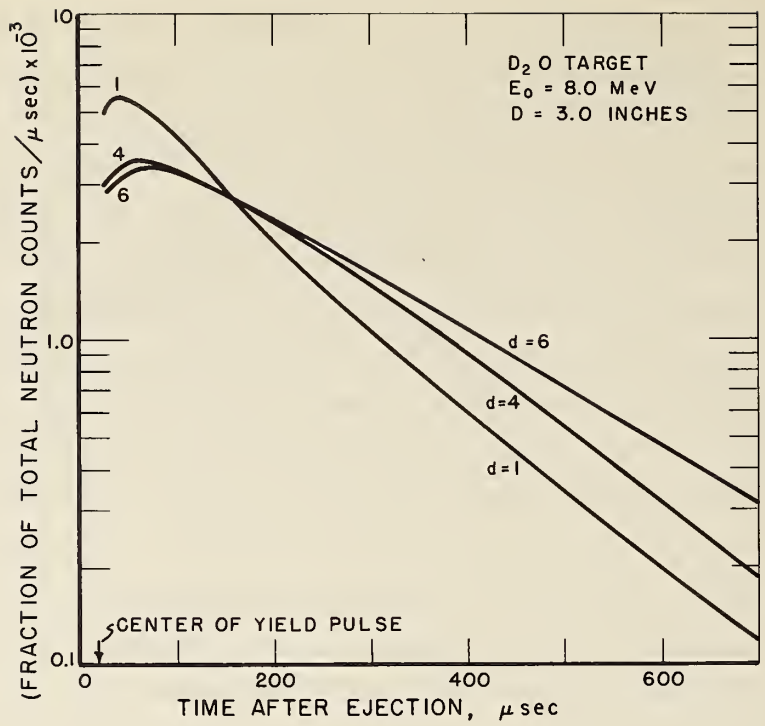


Fig. 19. Neutron time distribution. See discussion in text.

as changes in the gate factor. When gating after the yield pulse, the gating factor is particularly sensitive to small shifts in the gate opening since the fractional number of neutrons per μsec after the yield pulse is a maximum.

The influence of one counter on another counter in the oil bath was studied, using a RaDBe(α,n) source, in the geometry shown in Fig. 23. The neutron source was placed half-way down the beam tube but slightly below the beam tube axis. A counter, designated as A and shown in Fig. 24, was placed in a stationary position parallel to the beam tube such that there were 6 inches of oil moderator between it and the source. The neutron counting rate was recorded in A as a second counter designated as B, was paraded in a plane parallel to the tub wall on either side of A. The result of these measurements are given in Fig. 24; the value given at A was the counting rate of A when B was out of the moderator and the values given at various positions of B were the counting rates of A when B was in one of the given positions. The counting rate of A increased when B was between the source and A because B replaced mineral oil which would normally absorb neutrons. The counting rate of A was found to decrease for measurements made with B between A and the tub wall because the presence of B now meant the removal of oil which would normally scatter neutrons back to the counter.

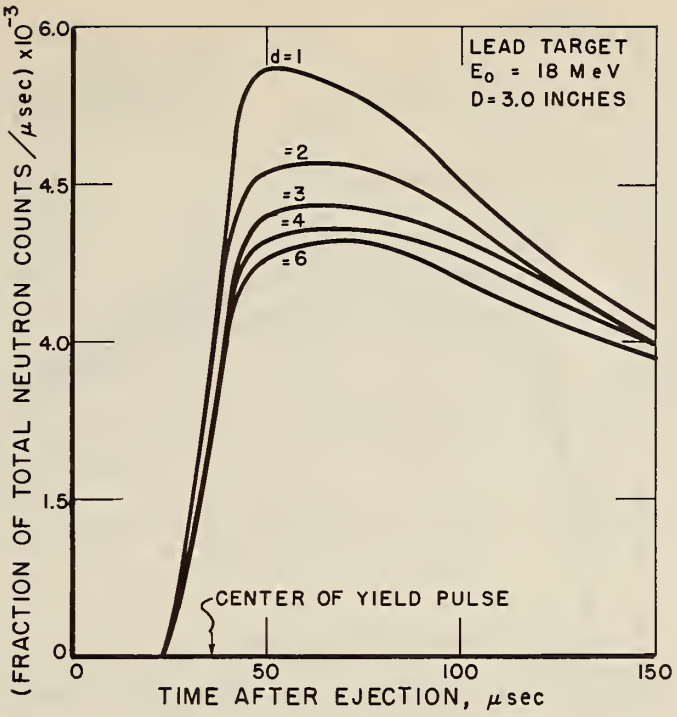


Fig. 20.

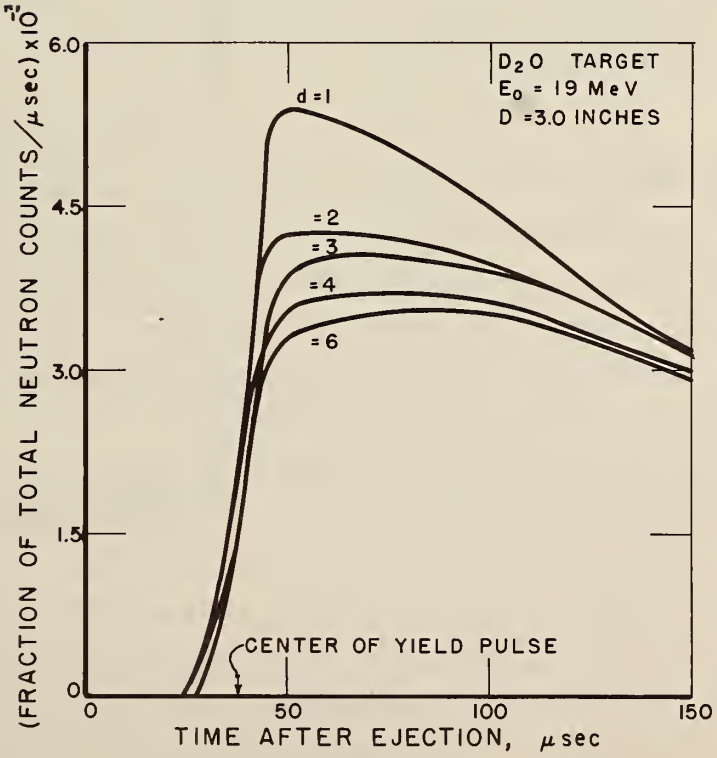


Fig. 21.

Figs. 20 & 21. Neutron time distribution on a linear scale. See discussion in text.

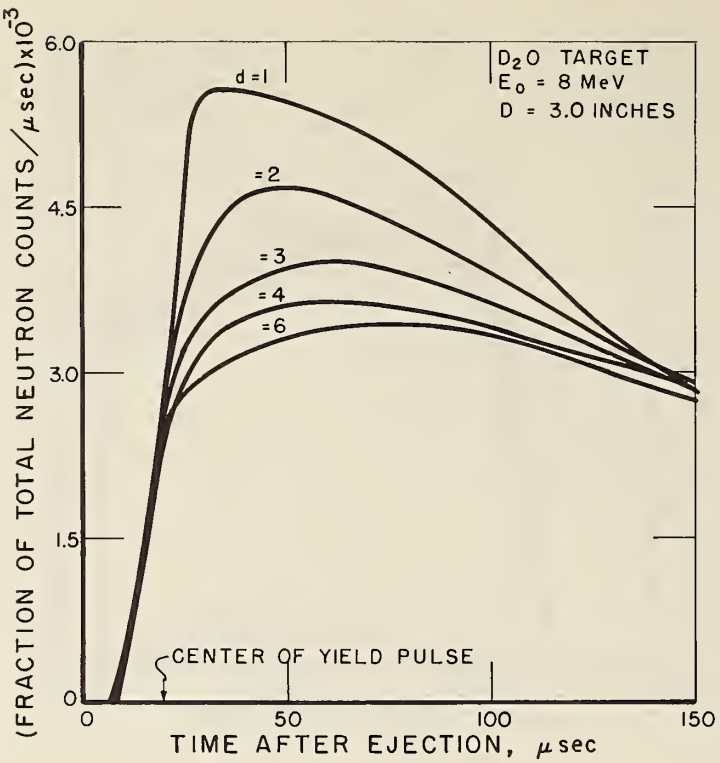


Fig. 22. Linear plot of the time distribution shown in Fig. 19. See discussion in text.

These effects were the greatest when B was in the plane determined by A and the source. These data indicate that counters of these dimensions (2-inch diameter, 15.7-inch active length) can be considered to respond independently of each other if there is at least 1 inch of moderator between adjacent counters arranged such that one is above or below the other (See Fig. 24). Further data, shown in Fig. 25, indicate a similar response if there are at least 2 inches of moderator between adjacent counters arranged such that one is in the shadow of the other.

The spacial distributions of neutrons within the moderator bath were measured by counting neutrons with a $BF_3$ counter at various positions in the tub. The experimental geometry and the position of the RaDBe(α,n) source was the same as that shown in Fig. 23. Although the geometry was far from ideal for this type of experiment, some indication of the counting rate decrease with moderator thickness was obtained and is shown in Fig. 26 where the numerical values given are the counting rates recorded by the counter at the given positions. A plot of the data taken in the horizontal plane through the axis of the beam tube decreased approximately exponentially. (See Fig. 27.)

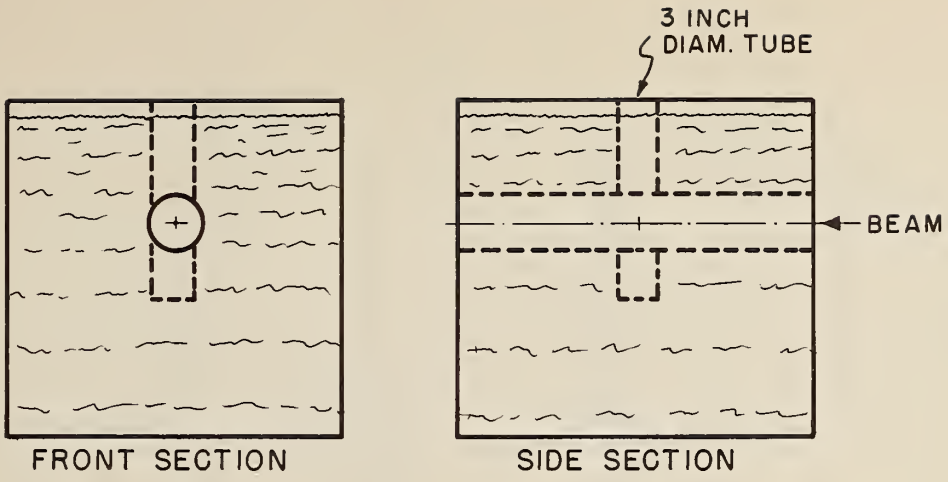


Fig. 23. Geometry used to study the influence of one counter on another counter.

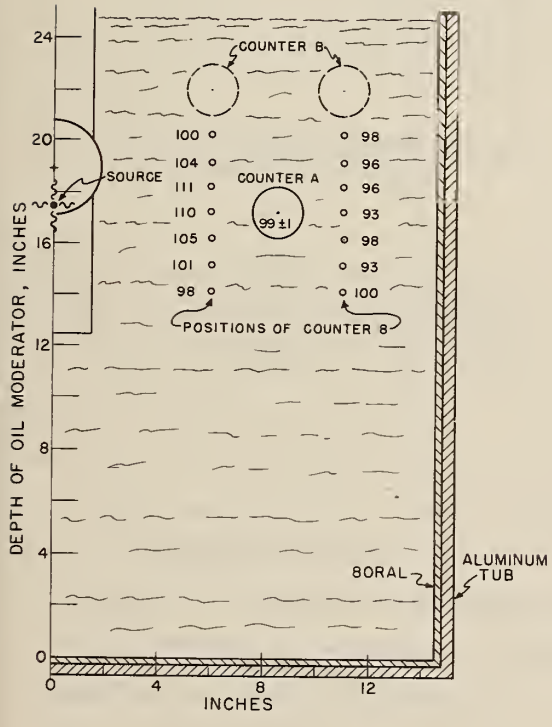


Fig. 24.

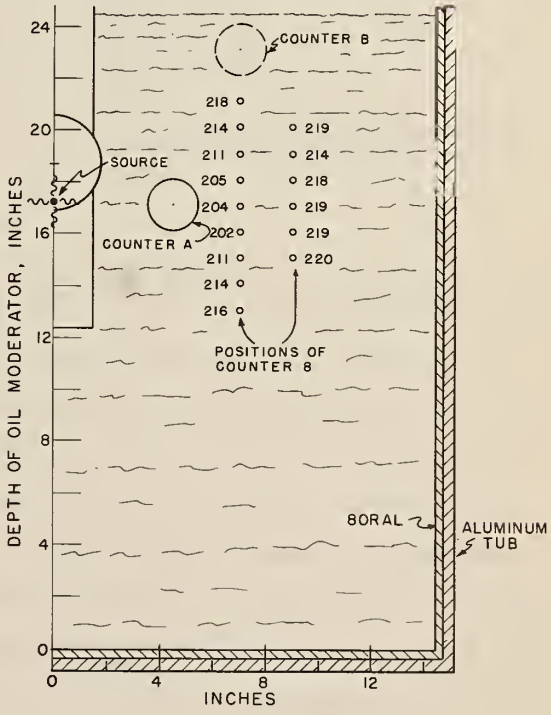


Fig. 25.

Figs. 24 & 25. Influence of neighboring counters on the response of a fixed counter.

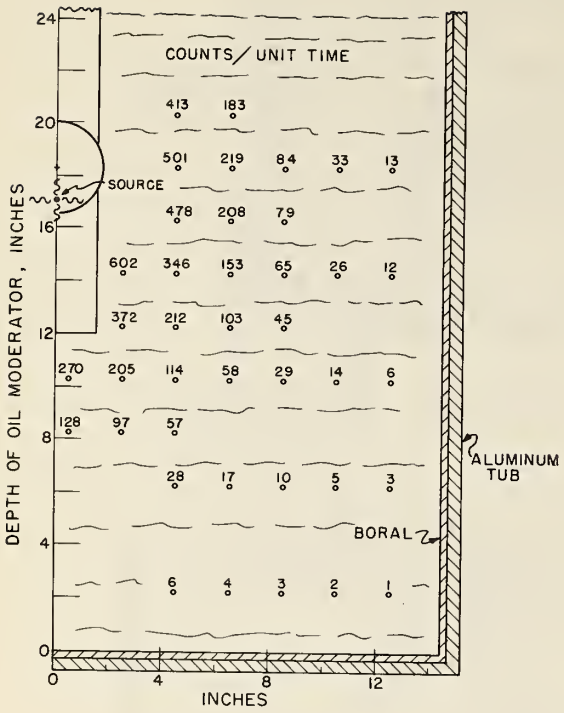


Fig. 26. The spacial distribution of neutrons from a RaDBe(α,n) source.

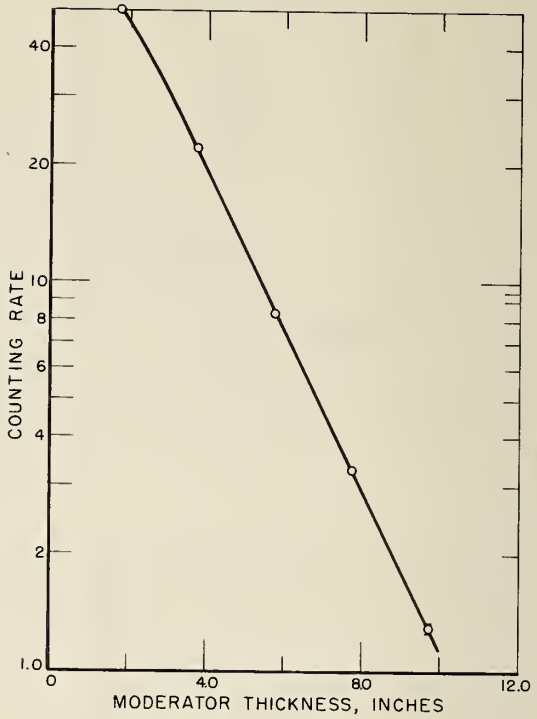


Fig. 27. Neutron counting rate versus moderator thickness as measured with the RaDBe(α,n) source. The data are from Fig. 26 taken in a horizontal plane through the axis of the beam tube.

Shielding of the neutron counters against neutrons produced by cosmic rays, an adjacent synchrotron, and the betatron itself was accomplished, as mentioned in Section II, by using both boral and borax shielding. The mineral oil itself also acted as a very good shield. Fig. 28 shows that for a $BF_3$ counter placed below 4 inches of oil, the background counting rate was reduced a factor of 10 of that with the counter at the surface of the oil. A combination of boral, borated paraffin, and paraffin placed around the aluminum moderator container was found to reduce the background anywhere from a factor of 2 to 5, depending on the depth of the counters in the mineral oil moderator.

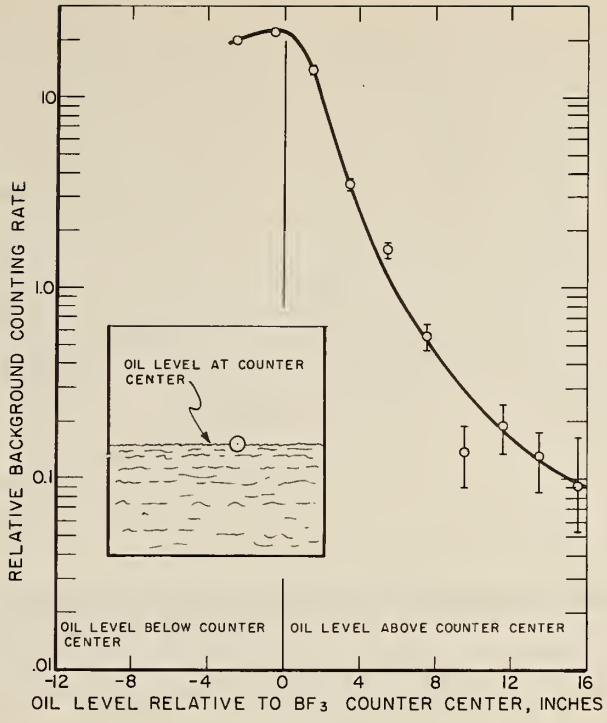


Fig. 28. Background counting rate versus oil moderator level.

### 5. Attenuation and Moderation in Samples

In order to determine the absolute yield per nucleus from measurements made of the neutron yield from samples of finite dimensions, it was necessary to make corrections for the effects that can take place in the samples themselves. The most important of these were: (1) the attenuation of the bremsstrahlung beam as it passes through the sample and (2) the moderation and absorption of the photoneutrons in the sample. These effects can be particularly important when the yields are measured for thick samples of low atomic weight materials.

For a bremsstrahlung spectrum given by $I(E,E_o)dE/E$, the number of neutrons counted per nucleus/cm$^2$ in the photon beam is given by:

$$Y(E_o) = \bar{\epsilon}\, M(E_o,t) \int_o^{E_o} \frac{\sigma_{tn}\, I(E,E_o)}{E}\, T(E,t)dE \qquad (6)$$

$$T(E,t) = \frac{\left[1 - e^{-\mu(E)t}\right]}{\mu(E)t}$$

where $\sigma_{tn} = \sigma(\gamma,n) + \sigma(\gamma,+n) + 2\sigma(\gamma,2n) + \ldots\ldots\ldots\ldots\ldots$ is the neutron production cross section, T(E,t) is a correction for the attenuation of the photon beam in the sample of thickness t, $\mu(E)$ is the photon attenuation coefficient, $\bar{\epsilon}$ is the mean neutron detection efficiency and $M(E_o,t)$ is a function to correct $\bar{\epsilon}$ for the moderation and absorption of the neutrons in the sample. For reasonably thin samples and for the heavier nuclei the function T(E,t) is essentially independent of the photon energy E. It can be removed from under the integral sign and evaluated at the mean photon energy absorbed by the nucleus. In the case of the calculated deuterium yields the dependence of T(E) on E was explicitly taken into account. For all other samples the dependence of T on the photon energy was negligible (less than 3% between the $(\gamma,n)$ thresholds and the peak bremsstrahlung energies used).

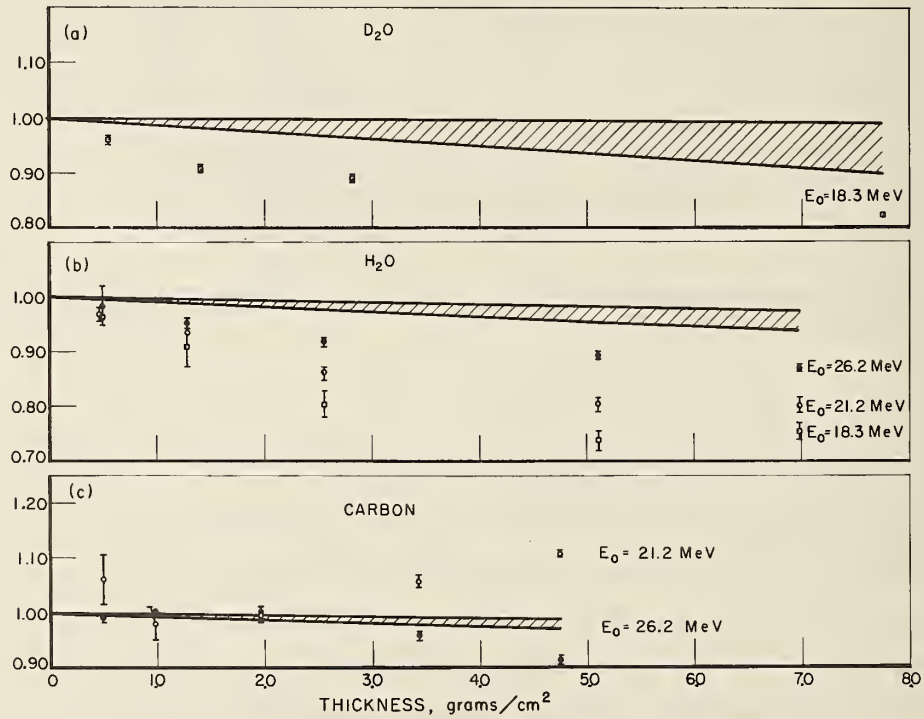


Fig. 29. Comparison of calculated and measured neutron yields per unit target thickness versus target thickness. The data have been arbitrarily normalized such that the extrapolated yield at zero target thickness is approximately equal to one. The two curves indicated in each subfigure represent the calculated yields using the total attenuation coefficient in Eq. 6 (lower curve) and that obtained calculated assuming that the Compton cross section did not contribute to the photon attenuation coefficient (upper curve). The diameter of the $D_2O$ and $H_2O$ targets was 2.0 inches while that of the carbon target was 1.75 inches.

For most of the nuclei studied the $(\gamma,n)$ thresholds are high and the total photon attenuation coefficient (Compton scattering plus pair production cross sections) is the proper quantity to use for $\mu(E)$. This is not the case for the $D_2O$ samples where Compton scattering is the dominant factor in the attenuation coefficient. Since this cross section is strongly peaked in the forward direction and since many of the scattered photons have energies above the $(\gamma,n)$ threshold in deuterium, only

a fraction of the total attenuation coefficient is effective in removing photons from the incident beam (for 10 MeV photons only about 50% of the scattered photons have energies below 2.2 MeV).

For the light nuclei the absolute neutron yield (neutrons per MeV of beam energy per nucleus per $cm^2$) was determined from an extrapolation to zero target thickness of the measured yields per unit thickness. The results of these measurements for targets of $D_2O$, $H_2O$, and carbon, using various bremsstrahlung energies, are shown in Fig. 29. In all cases, the data have been arbitrarily normalized such that the extrapolated yield at zero target thickness is approximately equal to one. The two curves indicated in each subfigure represent the calculated yields using the total attenuation coefficient in Eq. 6 (lower curve) and that obtained assuming that the Compton cross section did not contribute to the photon attenuation coefficient (upper curve).

If neutron moderation and absorption effects were not occurring the experimental points for the $D_2O$ data should fall somewhere between the two solid lines in Fig. 29-a. The point calculated for a target 7.76 $g/cm^2$ thick is 0.92 if only that part of the Compton cross section that results in scattered photons with energies below 2.2 MeV is used in $\mu(E)$. The difference between the experimental value and the expected value represents the effects of moderation and absorption occurring in the $D_2O$ target.

Both the direction and magnitude of this moderation effect are consistent with results obtained when the RaDBe($\alpha$,n) source was placed in a cell containing either $D_2O$ and $H_2O$. For the $H_2O$ data, shown in Fig. 29-b, the experimental points should be compared with the lower curve since even the highest energy photon used when scattered through an angle greater than 10 degrees loses enough energy to be below the ($\gamma$,n) threshold in $^{16}O$. The data obtained with the lower energy bremsstrahlung spectra indicate that the moderation effect is strongly dependent on the neutron spectrum. This correction would probably not affect the shape of the curve in Fig. 15 appreciably since the $H_2O$ source used was relatively thin in a direction perpendicular to the bremsstrahlung beam. On the other hand, the correction could effect the data for low energies plotted in Fig. 14 appreciably since the diameter of the $D_2O$ sample was the same as that used for these measurements. The shapes of curve indicated by the data points in Fig. 14 should therefore only be considered to give a qualitative indication of how the efficiency varies with neutron spectrum shape.

The measurements using a carbon target are shown in Fig. 29-c. As in the case of the $^{16}O$ measurements, the experimental points should be compared with the lower curve as almost all the photons that Compton scatter will have their energy reduced below the ($\gamma$,n) threshold. The data taken at 21.2 MeV are above this curve and are inconsistent with the measurements made with other samples. The cause of this discrepancy is not understood. It may be connected with the low ($\gamma$,n) and (n,2n) thresholds in $^{13}C$. At $E_o$ = 21.2 MeV, a large fraction of the neutrons from a carbon sample are due to the $^{13}C(\gamma,n)$ reaction. In any event, the effect points out the need for caution in

analyzing data obtained using thick targets in a Halpern-type detector.

Similar measurements were made with aluminum, silver, and gold targets. As was expected, the measured yield curves agreed with those calculated using the total photon attenuation coefficient.

### 6. Final Detector and Determination of Absolute Yields

Based on the previous measurements, a final detector was constructed in order to determine a number of absolute neutron yields. This detector had a moderator thickness (d) of 4 inches between the counters and a beam tube diameter (D) of 3 inches. Thirteen $BF_3$ counters were arranged on the circumference of a circle around the beam tube center such that there was a spacing of one inch between adjacent counters. The electronic and counting arrangements were essentially the same as that described in Section II.

The absolute efficiency of this detector was determined as a function of neutron source. The $d(\gamma,n)p$, $^{16}O(\gamma,n)^{15}O$, $^{31}P(\gamma,n)^{30}P$, and RaDBe(α,n) sources were used to make the measurements; these sources are described in Section III and their dimensions are given in Table 2. Except for target thickness corrections, the measurements were carried out as previously described. Because of its small dimensions, it was not felt necessary to make any corrections for finite sample size in the measurements made to determine the neutron detection efficiency with the $^{16}O(\gamma,n)^{15}O$ reaction. It was necessary to make these corrections in the latter measurements made with the larger samples to determine the absolute photoneutron yield. The uncertainties in the measurements are listed in Table 5.

Table 5. Uncertainty in the factors used to obtain the neutron detector efficiency.

| FACTOR | Target | $^{31}P$ | $D_2O$ | $^{16}O$ | $^{18}O$ | RaDBe(α,n) |
|---|---|---|---|---|---|---|
| | $E_o$ | 17.4 MeV | 18.3 MeV | 21.4 MeV | 24.5 MeV | |
| Counting statistics | | 1.1% | 0.3% | 2.8% | 2.2% | 0.4% |
| Gate | | 0.6% | 0.6% | 0.6% | 0.6% | - |
| Target purity | | - | 0.5% | - | - | - |
| Extrapolation for zero thick target yield | | - | 2.0% | - | - | - |
| Monitor calibration | | - | 1.1% | - | - | - |
| Calibration of betatron energy scale | | - | 0.32% | - | - | - |
| Photon spectrum shape | | - | 1% | - | - | - |
| Cross section | | - | 10% | - | - | - |
| Well crystal efficiency | | 3.2% | - | 3.2% | 3.2% | - |
| Decay constants | | 0.5% | - | 0.3% | 0.3% | - |
| Source strength | | - | - | - | - | 3.75% |
| Final estimated uncertainty | | 3.5% | 10.3% | 4.3% | 3.9% | 3.8% |

The uncertainty in the extrapolation to obtain the absolute neutron yield at zero target thickness was obtained from estimating the highest and lowest yield value obtained with different extrapolations consistent with the measured points. Uncertainties in the calibration of the well crystal are described in a later section. The influence of uncertainties in the photon spectral shape on the determination of the $D_2O$ efficiency were estimated by calculating the efficiency using the spectrum for zero angle [22] and comparing it with the result obtained with the integrated over the angle spectrum [11]. The difference in efficiency, which probably represents an extreme, was found to be less than 1% at 16.0 MeV. The final results of the detector calibration are shown in Fig. 30. The sources used in the final calibration can be divided into two groups: High energy RaDBe($\alpha$,n) and $^{16}O(\gamma,n)^{15}O$ ($E_o$ = 24.5 MeV), having a mean energy of about 4 MeV and low energy, $d(\gamma,n)p$ ($E_o$ = 18.3 MeV), $^{16}O(\gamma,n)^{15}O$ ($E_o$ = 21.4 MeV), $^{31}P(\gamma,n)^{30}P$ ($E_o$ = 17.4 MeV) having a mean energy of 2.0 MeV or less. The data of Fig. 30 indicate that the efficiency of the detector for these two groups of sources might be slightly different, 9.1% for the former and 10.1% for the latter. It should be pointed out that the usual photonuclear spectrum is probably much closer to that of the low energy sources used here. Only from some of the light nuclei would spectra similar to the high energy sources be obtained. For a photoneutron source of unknown spectral composition, the efficiency of the final detector is assumed to be (9.6± 0.5)%. The uncertainty quoted is assigned because of the possible variation of efficiency with spectral shape.

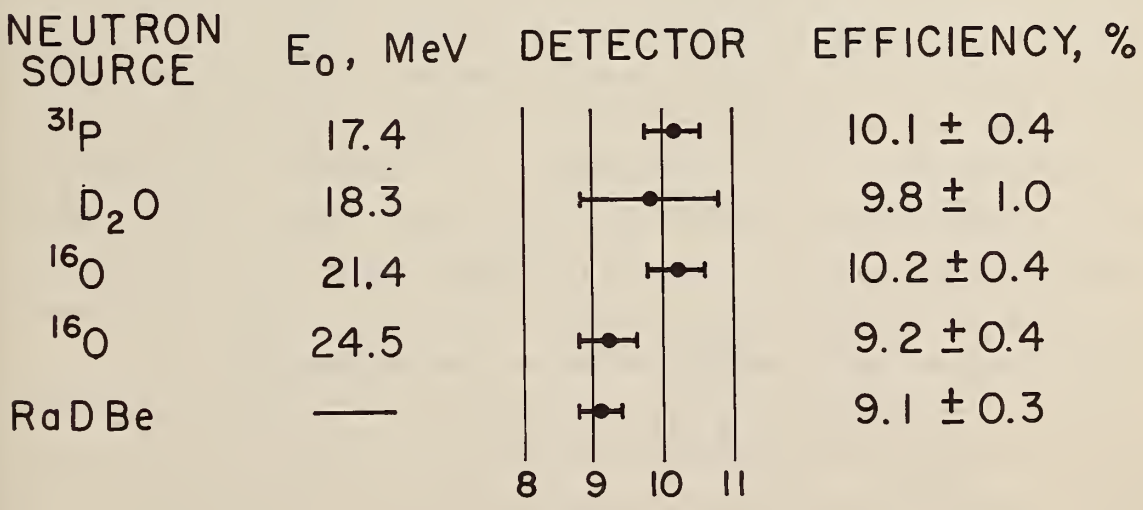


Fig. 30. Efficiency of the final detector as a function of neutron source. (Beam tube diameter 3.00 inches, moderator thickness 4.00 inches.) Estimated uncertainties are indicated.

The efficiencies determined with the water samples shed some light on the magnitude of the $^{16}O(\gamma,np)^{14}N$ cross section. If this reaction was occurring neutron emission would take place without the subsequent positron decay of the daughter nucleus. Since the detector efficiency was based on the ratio of neutron to positron counts, the efficiency would show an increase when measured above the $(\gamma,pn)$ threshold of $^{16}O$(23.0 MeV). The fact that no such increase is indicated in Figs. 15 or 30 can be taken as evidence that for an energy up to 28.9 MeV the integrated $(\gamma,np)$ cross section is small compared with the integrated $(\gamma,n)$ cross section.

The neutron yield from twelve elements throughout the periodic table was measured at peak bremsstrahlung energies ranging from 12 to 29 MeV. The experimental arrangement was the same as that described in Section II and shown in Fig. 5. The background was determined by measuring the neutron yield per unit monitor response with the target out of the detector. A comparison of the charge collected from the monitor chamber and the standard NBS ionization chamber, which was calibrated in terms of the photon beam energy incident on the front face, then gave the number of MeV of beam energy incident on the front face of the target. The absolute neutron yield, $Y(E_o)$, in units of neutrons per MeV per nucleus per $cm^2$, was then given by:

$$Y(E_o) = \frac{y(E_o)}{\varphi \epsilon n T(E_o,t)} \tag{7}$$

where $y(E_o)$ is the measured neutron yield per MeV of bremsstrahlung from n nuclei/$cm^2$, $\varphi$ is the gate factor, $\epsilon$ is the neutron detection efficiency and $T(E_o,t)$ is the correction for the finite thickness of the target. For all samples the neutron detection efficiency was taken to be (9.6± 0.5)%. The gate factor $\varphi$, or the ratio of the number of neutrons counted with a gate to those counted without a gate, was found to be 0.98 ± 0.005 for the 700μsec gate opening 10 μsec before the yield pulse.

The target thicknesses in $g/cm^2$, as given in Table 6, were determined by measuring the mass and area for all targets except holmium and oxygen. Because of its irregular shape, the $g/cm^2$ for holmium was obtained by measuring the mass, volume, and average thickness. The $g/cm^2$ for oxygen was determined from the target thickness and the known density of water. Within the uncertainties of the measurements the measured densities were consistent with handbook values [23].

The results of the neutron yield measurements are shown in Table 7 where the absolute neutron yield $Y(E_o)$ is given at peak bremsstrahlung energies of 27.0 and 22.0 MeV. The target out neutron yield was, in each case, less than 10% of the target in neutron yield. Fig. 31 shows how the absolute neutron yield varies as a function of Z at a peak bremsstrahlung energy of 27.0 MeV. For any given element the estimated uncertainty of the absolute yield points is of the order of 6% and is due to uncertainties in the counting statistics (0.5%), monitor comparison and absolute calibration (1.1%),

Table 6. Target properties.

| Target | Target Thickness $t(g/cm^2)$ | Target Thickness Correction Factor $\delta T(E_o,t)$ | Effective Nuclei/$cm^2$ $\frac{N_o t T(E_o,t)}{A} \times 10^{-23}$ |
|---|---|---|---|
| Carbon | 4.76 | 0.91($E_o$=26.2 MeV) | 2.17($E_o$=26.2 MeV) |
| Oxygen | 6.99 | 0.87($E_o$=26.2 MeV) | 2.03($E_o$=26.2 MeV) |
| Aluminum | 4.60 | 0.97 | 0.99 |
| Phosphorous | 6.25 | 0.95 | 1.15 |
| Calcium | 1.83 | 0.98 | 0.269 |
| Cobalt | 3.39 | 0.96 | 0.332 |
| Copper | 1.54 | 0.98 | 0.143 |
| Silver | 2.15 | 0.96 | 0.115 |
| Holmium | 5.66 | 0.87 | 0.180 |
| Tantalum | 1.69 | 0.95 | 0.0535 |
| Gold | 2.17 | 0.94 | 0.0623 |
| Lead | 2.04 | 0.95 | 0.0562 |

Table 7. Comparison of neutron yields. Yields are given in units of (neutron $cm^2$/MeV nucleus)$\times 10^{-28}$. The estimated uncertainties in Y and $Y_c$ are of the order of 6% and 10%, respectively.

| Element | $E_o$ | $Y(E_o)$ | $Y_c$ UCRL | $Y_c$ Saclay | $Y_c$ Va. | $Y_c$ NBS(Old) | $Y_c/Y$ UCRL Exp | $Y_c/Y$ Saclay Exp | $Y_c/Y$ Va. Exp | $Y_c/Y$ NBS(Old) Exp | Ref. |
|---|---|---|---|---|---|---|---|---|---|---|---|
| Pb | 27 | 103 | 86 | | | | 0.83 | | | | 26,30 |
| | 22 | 111 | 92 | 116 | | | 0.83 | 1.05 | | | |
| Au | 27 | 89 | 97 | | | | 1.09 | | | | 24,30, |
| | 22 | 92 | 98 | 88 | | 115 | 1.07 | 0.96 | | 1.25 | 38 |
| Ta | 27 | 81 | 82 | 77 | | | 1.01 | 0.95 | | | 27,30, |
| | 22 | 85 | 79 | 80 | | 113 | 0.93 | 0.94 | | 1.33 | 38 |
| Ho | 27 | 67 | 75 | | | | 1.12 | | | | 27,31, |
| | 22 | 69 | 77 | 82 | | 103 | 1.12 | 1.19 | | 1.49 | 39 |
| Ag | 27 | 36 | | | | | | | | | |
| | 22 | 34.8 | | | | | | | | | |
| Cu | 27 | 14.4 | 13.2 | | | | 0.92 | | | | 28,30 |
| | 22 | 12.6 | 11.5 | 12.4 | | | 0.91 | 0.98 | | | |
| Co | 27 | 12.7 | 12.1 | | | | 0.95 | | | | 29,34 |
| | 22 | 10.6 | 9.9 | | 13.5 | | 0.94 | | 1.27 | | |
| Ca | 27 | 1.69 | | 1.13 | 1.01 | | | 0.67 | 0.60 | | 32,35 |
| P | 27 | 2.35 | | | 1.76 | | | | 0.75 | | 36 |
| Al | 27 | 1.92 | 1.62 | | 1.38 | | 0.84 | | 0.72 | | 25,37 |
| $O^{16}$ | 27 | 0.54 | 0.42 | 0.48 | 0.42 | | 0.78 | 0.89 | | | 16,32, 37 |
| C | 27 | 0.50 | 0.35 | 0.33 | 0.46 | | 0.70 | 0.66 | | | 25,32, 33 |

gate factor (0.6%), number of target nuclei (1%), correction for the finite thickness of the target (2%), detector efficiency (5.0%), and the estimate of the betatron's peak bremsstrahlung energy. The uncertainty of the peak energy was determined to be less than 220 keV which, in the worst case, changed the absolute neutron yield by only 2%.

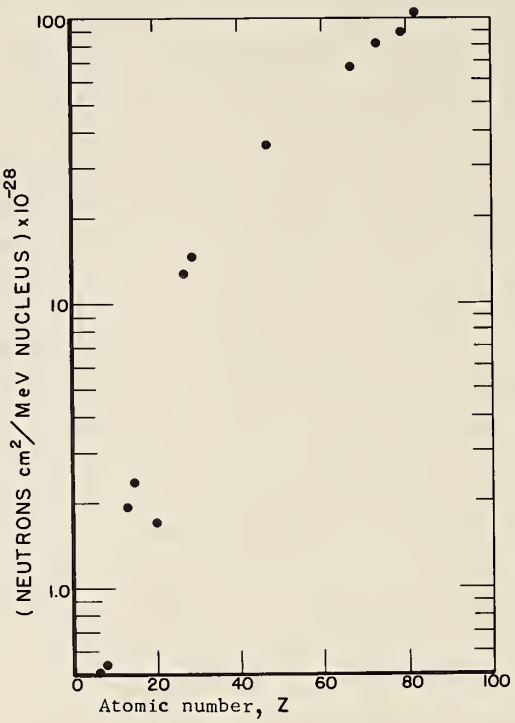


Fig. 31. Absolute neutron yield as a function of atomic number. The neutron yield from calcium (Z = 20) is particularly low in comparison with the other elements because its $(\gamma,n)$ threshold is high compared to the mean energy of the giant resonance.

The neutron yield from the high Z elements changed slowly with peak bremsstrahlung energy when operating at 22 MeV or higher. The yield at these energies was thus (1) insensitive to any reasonable variation in energy that might have occurred with the betatron and (2) not strongly dependent on the accurate knowledge of the betatron energy calibration. For these reasons it was meaningful to compare absolute yields for the high Z elements not only at 27 MeV but also at 22 MeV.

The neutron yields calculated from the cross sections measured at the Lawrence Radiation Laboratory, Saclay, University of Virginia, and the National Bureau of Standards, are compared with the present measurements in Table 7. The uncertainty in the calculated neutron yields resulting from the estimated uncertainties in the cross section is $\pm$ 10%. In order to facilitate a comparison the final

part of this table gives the ratios of the calculated yields to those measured in this work.

For the high Z elements, the calculated yields determined from the cross sections measured by the Lawrence Radiation Laboratory showed good agreement with the yields measured here except for lead which differed by 17%. A similar comparison, using the cross sections measured by the group at Saclay, showed excellent agreement for all elements except for holmium which differed by 19%. The only "heavy" element for which a comparison can be made with the Virginia group is cobalt. Here the yield calculated from their cross section data is 27% higher than the present measurements. The yields calculated from the previous NBS measurements are all high by factors that are quite consistent with the results of the present study. These early measurements were all made with a detector which had only three inches of paraffin moderator between the beam tube and the $BF_3$ counters. For such a detector the detector efficiency is about 20% lower for the RaDBe($\alpha$,n) spectrum used for calibration than for a "typical" photoneutron spectrum. (See Fig. 14 and discussion). In addition, the published holmium and lead cross sections [39,40] should be further reduced by 10% to correct for an erroneous gate factor that was used at the time the original data were analyzed [41].

For the low Z elements (calcium, phosphorous, aluminum, oxygen and carbon) the yields calculated from the published cross sections measured at other laboratories are all lower than these present measurements.

Although not shown in Table 7, a comparison was made of the experimental yield from carbon and the calculated yield from the data of Cook [42] who used a Halpern-type neutron detector with a moderator thickness of 10.3 cm. The agreement was excellent. A similar comparison was made using the recently measured $^{16}O(\gamma,n)^{15}O$ cross section of Cook et al. [43]. Good agreement was obtained. This measurement was obtained by detecting the residual activity.

In summary, the results of the experimental and calculated yields agree reasonably well for the high Z elements. For the low Z elements, where the neutron spectra change rapidly with energy, the agreement of experimental and calculated yields is, in general, very poor. This disagreement of cross section magnitudes for the light elements may be mainly a problem of the energy response of the neutron detectors used to measure the cross sections.

## Appendix 1. Determination of the Absolute Positron Efficiency

A schematic diagram of the detector and electronics used in the positron calibration of the NaI(Tl) crystal is shown in Fig. 32. The crystal was a 3x3 inch cylindrical well crystal having a well diameter of 0.75 inches and a well depth of 2.0 inches. The crystal was shielded in a lead hut having a minimum thickness of 4.0 inches; the inside surface of the hut was covered with 0.04 inches of cadmium, followed by 0.013 inches of brass in an attempt to reduce fluorescent radiation from the lead shield [44]. The signal from the cathode of the phototube went to a cathode follower and was then amplified and fed to a standard 256 channel pulse height analyzer.

A calibrated $^{22}Na$ source was used to determine the efficiency of the crystal for detecting positrons because it had a reasonably simple decay scheme and was readily available as an accurately calibrated source†. The source was obtained as a liquid solution sealed in a cylindrical glass vial. The liquid in the vial had a diameter of 0.62 inches and a height of 0.91 inches. In order to minimize the effects due to geometry, these dimensions were very nearly the same (±5%) as those of the water and phosphorous targets used during the absolute calibration of the neutron detector.

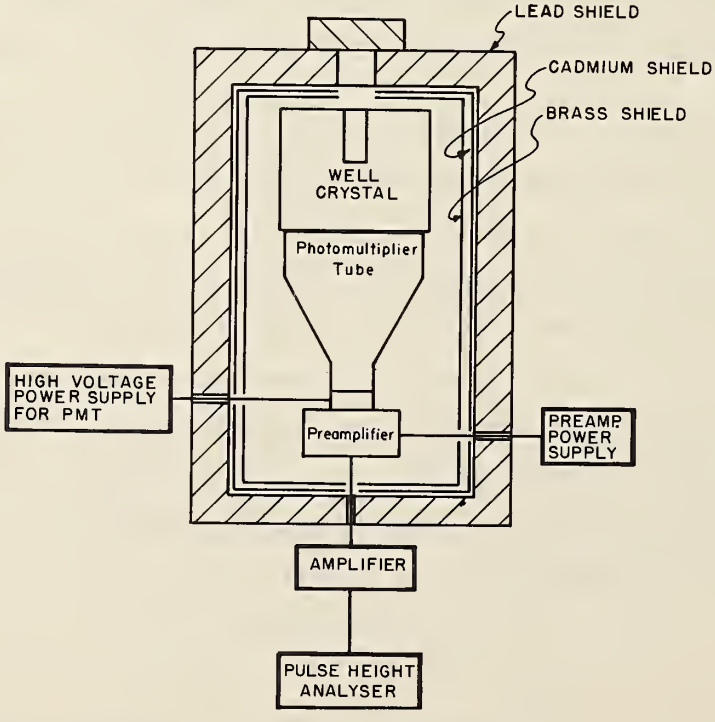


Fig. 32. A schematic diagram of the detector and electronics used for the positron calibration of the NaI(Tl) crystal. The cylindrical well crystal was shielded with a minimum thickness of 4.0 inches of Pb; the cadmium and brass shields were used to reduce fluorescent radiation from the lead shield.

†Supplied by the Radioactivity Section of the National Bureau of Standards.

The decay scheme of $^{22}Na$, which is shown in Fig. 33, is such that it decays to the 1.274 MeV excited state of $^{22}Ne$ by positron emission 89.8% of the time and by orbital electron capture 10.2% of the time. The NaI(Tl) crystal detected not only the positron annihilation radiation (0.511 MeV photons) but also the 1.274 MeV photons. Since the source to be counted with the crystal emitted positrons only, it was necessary to correct the counting rate observed with the $^{22}Na$ source for the additional counts resulting from the presence of this line. The pulse height spectrum obtained when counting the $^{22}Na$ source in the well crystal is shown in Fig. 34. The five major peaks were due to the 0.511 MeV positron annihilation photons and the 1.274 MeV photons interacting in the crystal either separately or in coincidence. The expression for the number of interactions that occurred in the crystal can be written as:

$$Q = f(\beta+)N_d \left\{ \varepsilon(\beta+) \left[1 - \varepsilon(1.27)\right] + \varepsilon(1.27) \left[1 - \varepsilon(\beta+)\right] + \varepsilon(1.27)\ \varepsilon(\beta+)\right\} + N_d\ \varepsilon(1.27)\left[1 - f(\beta+)\right] \tag{8}$$

where Q is the observed counting rate in the crystal, Nd is the disintegration rate of $^{22}Na$, $f(\beta+)$ is that fractional number of $^{22}Na$ disintegrations which decay by positron emissions [45], $\varepsilon(\beta+)$ is the probability that the crystal detects a positron, and $\varepsilon(1.27)$ is the probability that the crystal detects a 1.27 MeV photon. The first term in eq. 8 expresses the interactions in the crystal for the decay scheme which takes place by positron emission followed by photon emission and the second term expresses the interactions in the crystal for the decay scheme which takes place by internal conversion followed by photon emission.

Eq. 8 can be solved for $\varepsilon(\beta+)$:

$$\varepsilon(\beta+) = \frac{Q - Nd\ \varepsilon(1.27)}{f(\beta+)\ Nd\left[1 - \varepsilon(1.27)\right]} \tag{9}$$

where the only unknown is $\varepsilon(1.27)$.

The efficiency for detecting the 1.27 MeV photons, $\varepsilon(1.27)$, was obtained by first determining the crystal efficiency for detecting the 1.11 MeV photon from a calibrated $^{65}Zn$ source. For extrapolation purposes, the measured efficiency of the crystal can be expressed in terms of the photon attenuation coefficient and a mean crystal thickness defined by:

$$\varepsilon(E) = 1 - e^{-\mu(E)t} \tag{10}$$

where $\epsilon(E)$ is the crystal efficiency for detecting photons of energy E, $\mu(E)$ is the photon attenuation coefficient at photon energy E, and t is a mean crystal thickness in $g/cm^2$. From this equation, the effective $\mu t$ for 1.27 MeV photons was estimated from the expression:

$$\mu t(1.27) = \frac{\mu(1.27)}{\mu(1.11)} \mu t(1.11) \tag{11}$$

where $\mu(1.27)$ and $\mu(1.11)$ are the published mass absorption coefficients for 1.27 and 1.11 MeV photons. Using eqs. 9 and 10, $\epsilon(1.27)$ can be expressed as:

$$\epsilon(1.27) = 1 - \left[1 - \epsilon(1.11)\right]^{\mu(1.27)/\mu(1.11)} \tag{12}$$

The uncertainty in $\epsilon(\beta+)$, the positron efficiency of the crystal, was estimated to be ±3.2% and was primarily due to uncertainties in the source calibration (1%), the extrapolation of the pulse height distribution (1%) and the branching ratio (1%) for the disintegration of $^{22}Na$ source. Another possible uncertainty could have been caused by the fact that the response of the well crystal varied somewhat with the depth of the source in the well and the activity of the target could vary along the long axis of target due to attenuation of the bremsstrahlung beam. This effect was probably negligible for the water target as mixing (due to handling) occurred which distributed the activity evenly similar to that of the liquid $^{22}Na$ ccalibration source. With the solid phosphorous target, however, no mixing could occur. It was estimated that this caused an error of no more than 0.2% in the absolute efficiency of the neutron detector. The efficiency of the crystal was determined 5 times over a period of 7 months. The rms deviation of these determinations was 1% indicating that the reproducibility of the measurement was considerably better than the estimated 3.2% uncertainty given above.

The crystal efficiency for detecting positrons, $\epsilon(\beta+)$, was also determined, as a check on the measured value, by calculating $\epsilon(0.511)$ in a way similar to that used to obtain $\epsilon(1.27)$. This was then used to obtain $\epsilon(\beta+)$ from the following relationship:

$$\epsilon(\beta+) = 2\epsilon(0.511)\left[1 - \epsilon(0.511)\right] + \epsilon^2(0.511) \tag{13}$$

The difference between the two determinations of $\epsilon(\beta+)$ was less than 1.25%, well within the estimated uncertainties in the measurements.

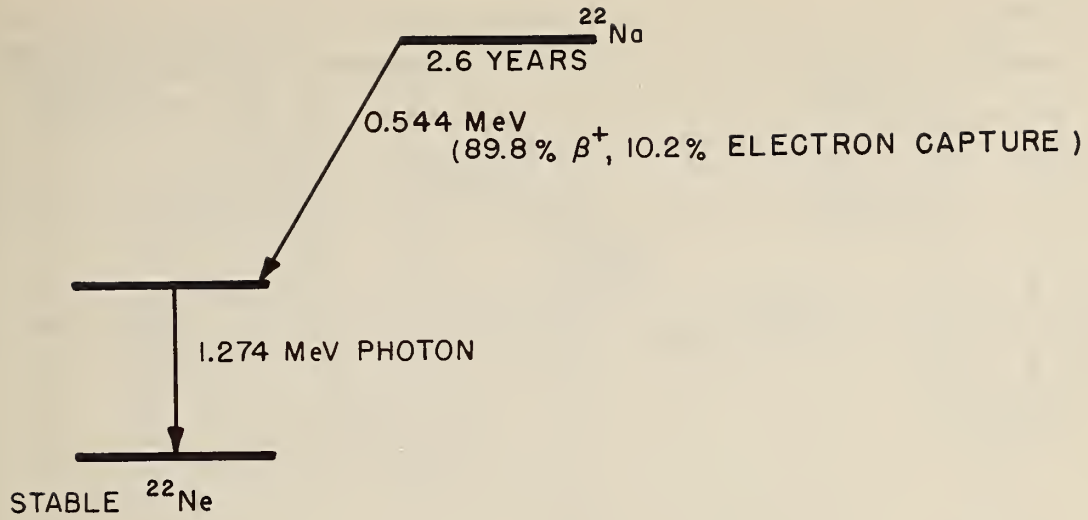


Fig. 33. The decay scheme of $^{22}Na$. Decay modes less than 0.06% are not shown.

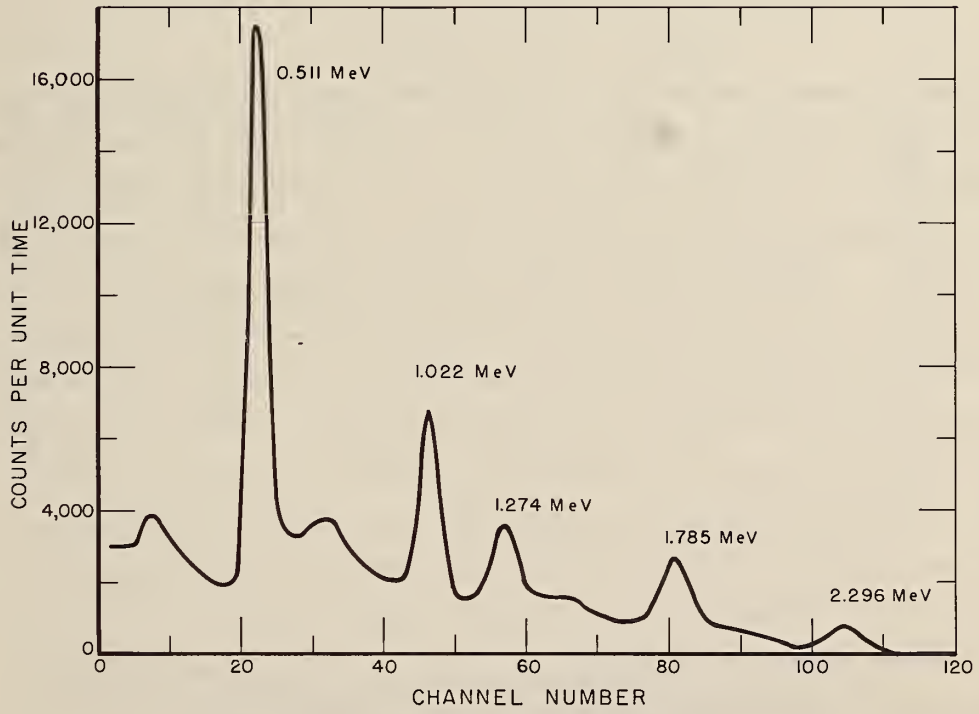


Fig. 34. The pulse height spectrum obtained when counting the $^{22}Na$ source in the NaI(Tℓ) well crystal. The five major peaks indicated are due to the positron annihilation radiation and the 1.274 MeV photons interacting in the crystal either separately or in coincidence.

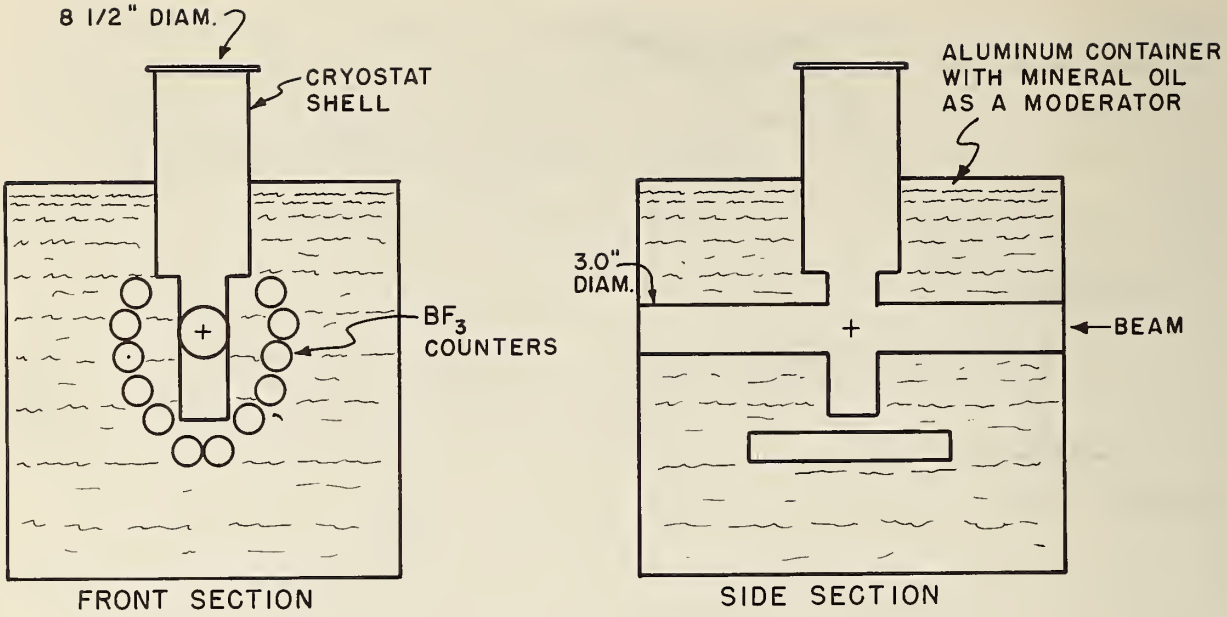


Fig. 35. Cryostat neutron detector.

Appendix 2. Cryostat Geometry

Fig. 35 shows the geometry that was used for an experiment in which a $^3$He refrigerator was used to cool a sample so that the neutron yield could be studied as a function of the orientation of the nucleus with respect to the photon beam direction [46]. The arrangement of the detectors in this case was determined primarily by the size and shape of the cryostat and the need for high detection efficiency. In order to obtain a detection efficiency that was uniform for a heavy nucleus photoneutron spectrum, an attempt was made to keep a minimum of approximately three inches of moderator between the neutron source and the midpart of any counter. Twelve $BF_3$ counters were arranged parallel to the beam tube below and to the side of the target. The moderator thickness between the target and the counter was 3 inches for the counters to the side of the target and 1 to 3 inches (the distance varied due to the smaller hole below the beam tube) for the counters below the target. A moderator thickness of 0.5 inches was used between any two adjacent walls.

Fig. 36 gives the efficiency for the crystal detector obtained using the d($\gamma$,n) source and the RaDBe($\alpha$,n) source. As was done for the data plotted in Fig. 14, the data taken with the $D_2O$ source were corrected for the finite thickness of the target by assuming that only half of the Compton cross section was effective in removing photons from the bremsstrahlung beam. Also shown in Fig. 36 are the data from Table 4 for a beam tube diameter of D = 3.0 inches. The two sets of data have been normalized to have the same efficiency for the RaDBe($\alpha$,n) source. On the basis

of this comparison, the cryostat detector would seem to have a detection efficiency that depends upon neutron energy very similar to that of a single counter having three inches of moderator between it and the source. (See Figs. 14, 15, 16 and the discussion in Section IV.) On the basis of the results given in Sections IV and VI, the true efficiency for detecting a photoneutron spectrum from a heavy nucleus with this detector was about 20% larger than the figure of 7.8% quoted in ref [46].

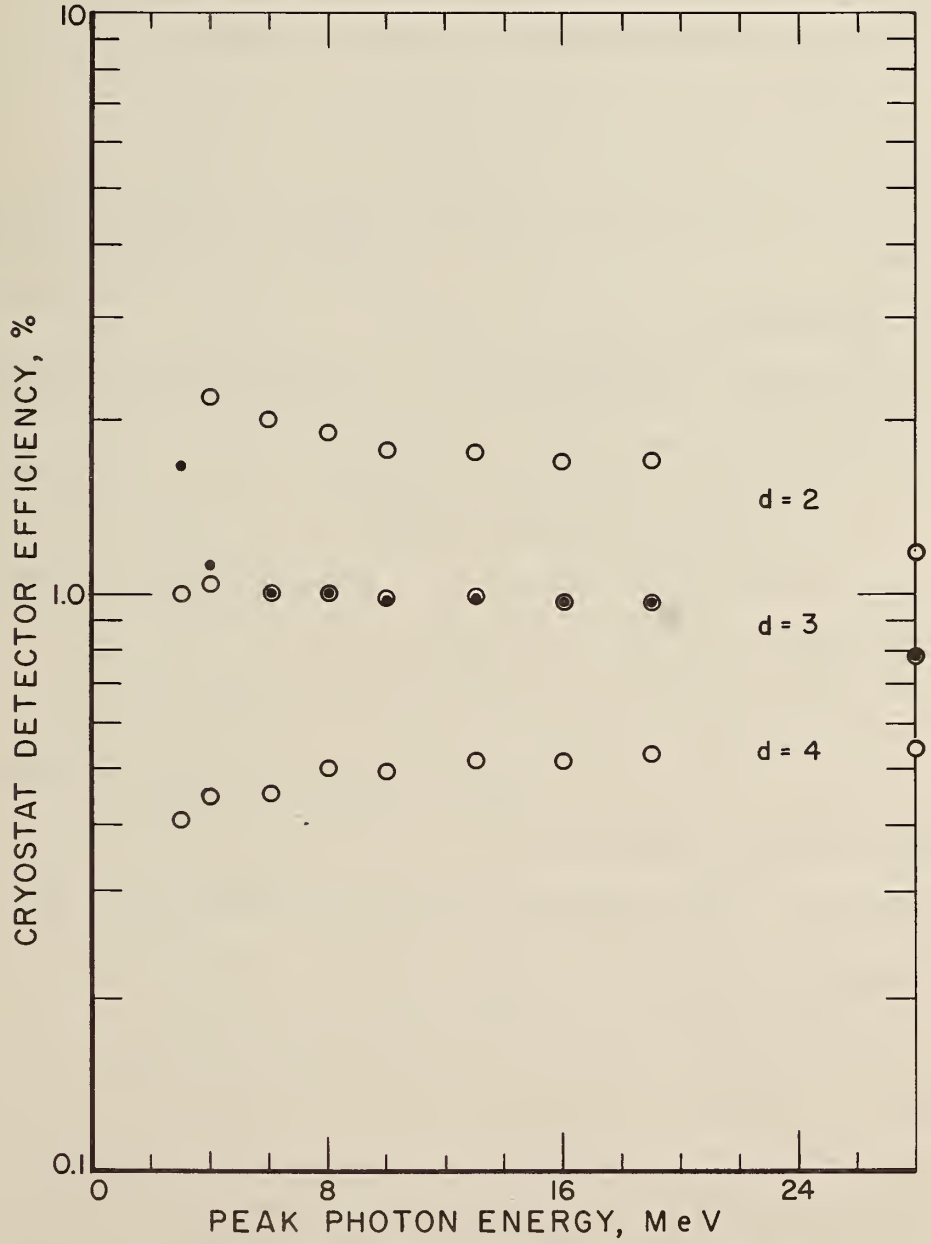


Fig. 36. Efficiency of the cryostat detector. The points along the right ordinate scale were determined with the RaDBe(α,n) source. Points indicated by solid circles were measured for the cryostat detector shown in Fig. 35. Points indicated by open circles are from Table 4 (D=3.0 inches). The two sets of data are normalized at the RaDBe(α,n) points.

## References


[1] J. Halpern, A. K. Mann and R. Nathans, Rev. Sci. Instr. 23, 678 (1952).

[2] B. B. Rossi and H. H. Staub, Ionization Chambers and Counters, 1st edition, (McGraw-Hill Book Company, Inc., 1949), p 192.

[3] R. W. Fast, P. A. Flournoy, R. S. Tickle and W. O. Whitehead, Phys. Rev. 118, 535 (1960).

[4] B. M. Spicer, H. H. Thies, J. E. Baglin and F. R. Allum, Australian J. Phys. 11, 298 (1958).

[5] J. E. Baglin, M. N. Thompson and B. M. Spicer, Nucl. Phys. 22, 207 (1961).

[6] F. R. Allum, G. M. Crawley and B. M. Spicer, Nucl. Phys. 51, 177 (1964).

[7] G. Holt, Arkiv. Fysik 8, 165 (1954).

[8] G. R. Hogg, University of Melbourne Report, UM-P-63/1.

[9] J. S. Pruitt and S. R. Domen, NBS Monograph 4B, (1962).

[10] NBS Handbook 72, (1960) Measurement of Neutron Flux and Spectra for Physical and Biological Applications.

[11] A. S. Penfold and J. E. Leiss, Physics Research Laboratory Report, University of Illinois, Champaign, Illinois (1958).

[12] E. G. Fuller and E. Hayward, Nuclear Reactions, edited by P. M. Endt and P. B. Smith (Amsterdam: North Holland Publishing Co., 1962), Vol. II, Chapter II, p 273.

[13] L. Hulthen and B. C. H. Nagel, Phys. Rev. 90, 62 (1953).

[14] J. J. de Swart and R. E. Marshak, Physica 25, 1001 (1959).

[15] K. N. Geller and E. G. Muirhead, Phys. Rev11, 371 (1963).

[16] J. T. Caldwell, R. R. Harvey, R. L. Bramblett and S. C. Fultz, Phys. Rev. 6, 213 (1963).

[17] Private communication, F. W. F. Firk, October 1966.

[18] A. S. Penfold and E. L. Garwin, Rev. Sci. Instr. 31, 155 (1960).

[19] E. Hayward and T. Stovall, Nucl. Phys. 69, 241 (1965).

[20] R. Meads, C. England, C. Collie and G. C. Weeks, Proc. Phys. Soc. (London) 69, 469 (1956).

[21] Beta- and Gamma- Ray Spectroscopy, K. Siegbahn, ed., (North Holland Publishing Co., Amsterdam 1955) 1st ed., Appendix I, pps 857-874.

[22] NBS Handbook 55 (1954), Protection Against Betatron-Synchrotron Radiations up to 100 Million Electron Volts.

[23] Handbook of Chemistry and Physics, C. D. Hodgman, R. C. Weast, S. M. Selby, editors, (Chemical Rubber Publishing Co., Cleveland, Ohio, 1956) 38th ed.

[24] S. C. Fultz, R. L. Bramblett, J. T. Caldwell and N. A. Kerr, 127, 1273 (1962).

[25] S. C. Fultz, J. T. Caldwell, B. L. Berman, R. L. Bramblett and R. R. Harvey, Phys. Rev. 143, 790 (1966).

[26] R. R. Harvey, J. T. Caldwell, R. L. Bramblett and S. C. Fultz, Phys. Rev. 136, B126 (1964).

[27] R. L. Bramblett, J. T. Caldwell, G. F. Auchampaugh and S. C. Fultz, Phys. Rev. 1129, 2723 (1963).

[28] S. C. Fultz, R. L. Bramblett, J. T. Caldwell, and R. R. Harvey, Phys. Rev. 133, B1149 (1964).

[29] S. C. Fultz, R. L. Bramblett, J. T. Caldwell, N. E. Hansen and C. P. Jupiter, Phys. Rev. 128, 2345 (1962).

[30] J. Miller, G. Schuhl, and C. Tzara, Nucl. Phys. 32, 236 (1962).

[31] P. Axel, J. Miller, C. Schuhl, G. Tomas, C. Tzara, J. de Physique et Rad. 27, 262 (1966).

[32] J. Miller, C. Schuhl, G. Tomas and C. Tzara, Phys. Letters 2, 76 (1962).

[33] K. Min and W. D. Whitehead, Phys. Rev. 137, B301 (1965).

[34] P. A. Flournoy, R. S. Tickle and W. D. Whitehead, Phys. Rev. 120, 1424 (1960).

[35] K. Min, L. N. Bolen and W. D. Whitehead, Phys. Rev. 132, 749 (1963).

[36] L. N. Bolen and W. D. Whitehead, Phys. Rev. 132, 2251 (1963).

[37] L. N. Bolen and W. D. Whitehead, Phys. Rev. Letters 9, 458 (1962).

[38] E. G. Fuller, M. S. Weiss, Phys. Rev. 112, 560 (1958).

[39] E. G. Fuller, E. Hayward, Nucl. Phys. 30, 613 (1962).

[40] E. G. Fuller, E. Hayward, Nucl. Phys. 33, 431 (1962).

[41] Private communications, E. G. Fuller and E. Hayward (1966).

[42] B. C. Cook, Phys. Rev. 106, 300 (1957).

[43] B. C. Cook, J. E. E. Baglin, J. N. Bradford and J. E. Griffin, Phys. Rev. 143, B712 (1966).

[44] Methods of Experimental Physics, L. Marton, ed., (Academic Press Inc., New York, 1961) 1st ed., Vol. V., Part A, Chap. 2, p 631.

[45] Nuclear Data Sheets, compiled by K. Way et al. (Printing and Publishing Office, National Academy of Sciences - National Research Council, Washington 25, D. C. 1961) NRC 59-4-16.

[46] E. Ambler, E. G. Fuller and H. Marshak, Phys. Rev. 138, B117 (1965).

* U.S. GOVERNMENT PRINTING OFFICE: 1967—251-027/120

U.S. DEPARTMENT OF COMMERCE
WASHINGTON, D.C. 20230

OFFICIAL BUSINESS

POSTAGE AND FEES PAID
U.S. DEPARTMENT OF COMMERCE